博　士　論　文

Assembly domain-based optogenetic system for the efficient control of cellular signaling

(細胞内シグナル伝達の高効率な操作を実現する
自己集合型光遺伝学システム)

古谷　昭博

Assembly domain-based optogenetic system for the efficient control of cellular signaling

A dissertation submitted to the University of Tokyo
for the degree of Doctor of Arts and Sciences

by **Akihiro FURUYA**

Acknowledgements

At first, I would like to make a most cordial acknowledgment to Associate Professor Dr. Moritoshi Sato for his strict leadership and instructions, at the same time, his lively nature, which replenished me to accomplish the precious scientific works in fulfilling atmosphere.

I would like to express my deep thanks to Dr. Takahiro Nakajima for cooperating me to achieve difficult measurements without feeling tedious and for helping me to understand my own study deeper and from various viewpoints.

I gratefully acknowledge Dr. Yoshibumi Ueda with deep appreciation for working cooperatively with me to write my virgin paper. He taught me what the scientific paper should be. In addition, in soccer games, I shared diverting times with him together.

Further thanks go to:

Mr. Aono gave me a number of assistance for using various microscopies.

Mr. Nihongaki has inspired me by his vast biological knowledge.

Mr. Yu has provided encouragement for me by his happy personality.

Thanks to all other students of Prof. Sato's laboratory for their kind assistance.

Abstract

Our laboratory previously developed the Magnet system, which consists of two distinct Vivid protein variants, one positively and one negatively charged, designated the positive Magnet (pMag) and negative Magnet (nMag), respectively. These two proteins bind to each other through electrostatic interactions, preventing unwanted homodimerization and providing selective light-induced heterodimerization. The Magnet system enables the manipulation of cellular functions such as protein-protein interactions and genome editing, although the system could be improved further. In order to enhance the ability of pMagFast2 (a pMag variant with fast kinetics) to bind nMag, I introduced several pMagFast2 modules in tandem into a single construct, pMagFast2(3×). However, the expression level of this construct decreased drastically with increasing number of pMagFast2 molecules integrated into a single construct. In the present study, I applied a new approach to improve the Magnet system based on an assembly domain (AD). Among several ADs, the Ca^{2+}/calmodulin-dependent protein kinase IIα association domain (CAD) most enhanced the Magnet system. The present CAD-Magnet system overcame a trade-off issue between the expression level and binding affinity. The CAD-converged 12 pMag photoswitches exhibited a stronger interaction with nMag after blue light irradiation compared with monomeric pMag. Additionally, the CAD played a key role in converging effector proteins as well in a

single complex. Owing to these substantial improvements, the CAD-Magnet system combined with Tiam1 allowed us to robustly induce localized formation of vertical ruffles on the apical plasma membrane. The CAD-Magnet system combined with 4D imaging was instrumental in revealing the dynamics of ruffle formation.

Table of Contents

Chapter I

General Introduction

I-I Advent of optogenetics

A cell, a unit of life, is a biological computer. It receives various small molecules, including ions, peptides, and proteins, as complex input signals from both within and outside of itself. Then it processes them and generates output signals by activating the appropriate mechanisms. To understand the input/output mechanisms of cells, it is necessary to study the behavior of these molecules as well as the timing, the position and the mechanism of their action. Elucidating the dynamics of these molecules within cells is important for answering many questions in the life sciences and medicine, particularly those pertaining to disease and therapy. One analytic approach to understanding the role of these molecules is to perturb cells and carefully examine their responses. In particular, “chemically inducible dimerization” (CID) was developed to conduct perturbation studies[1]. In CID, FK506-binding protein (FKBP) and FKBP12-rapamycin-associated protein (FRB), which dimerize in the presence of rapamycin, are expressed as fusions with proteins of interest (**Fig. 1-1**). The addition of rapamycin to cells induces the cellular functions mediated by the proteins of interest fused with FKBP and FRB respectively. These functions include translocation of a specific protein to the specific membrane and association of one protein with another. This technique allows temporal manipulation of the activity of specific proteins, thereby providing insights into the roles of various proteins and their reaction kinetics in cellular signaling. Such information cannot be obtained by conventional methods,

including ligand stimulation or gene knock-in/knock-out. However, inherent drawbacks, such as toxicity along with rapid diffusion and persistence of the inducers, limit the applicability of CIDs.

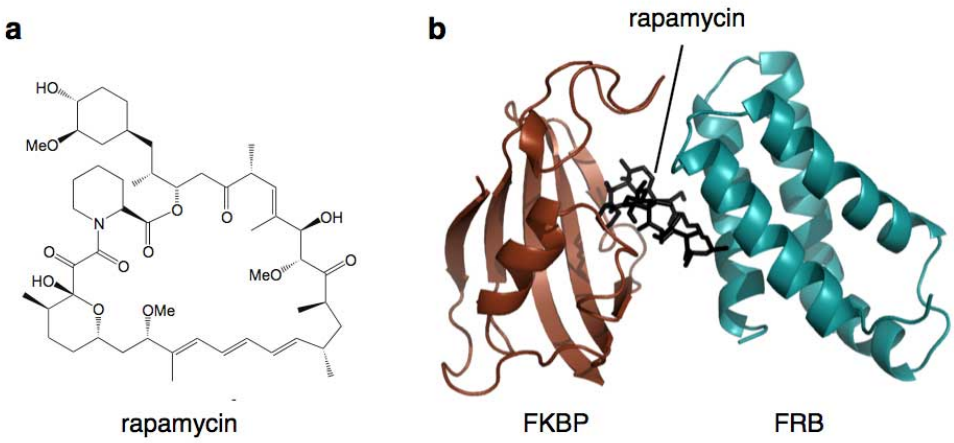

Figure 1-1. The structures of rapamycin **(a)** and FKBP-rapamycin-FRB complex **(b)**. In the presence of rapamycin, FKBP and FRB make complex. This behavior can be used to induce protein-protein interaction.

In the last decade, optics and genetics have been merged into “optogenetics”, which is a technology for developing systems that induce cellular functions with light[2]. Compared to chemical systems, optogenetic systems activated with light show high spatial-temporal resolution and do not generally require the addition of chemical compounds that might perturb the intact cellular systems. The characteristics of light provide us with new possibilities for controlling well-defined events in biological systems at the subcellular point and at the time at will. Under these regulations, the cell systems are kept in the native condition, thereby biological events inside are clearly

understood without disturbance. The first optogenetic tools were photo-sensitive chemically caged inducers. Those were maintained in an inactive state by a light-cleavable group. Chemically caged molecules divide under irradiation with UV light, as photo-sensitive molecules eject in an active state. Photo-sensitive molecules prepared in this way harbor chemical inducers, nucleic acids and transcription factor[3]. However, an apparent drawback of this method is the need of either synthesis of the caged molecules outside the cells or modification of the genetic code for proteins to be assembled from caged amino acids. On the other hand, microbial opsin and melanopsin have been applied as optogenetic systems in neuroscience over the last few years[4,5]. Microbial opsins have the non-selective permeability to cations under blue light exposure[6] (**Fig. 1-2**), and melanopsins are activated by an influx of calcium through ion channels, which excites a GTPase signaling pathway[7]. Opsins have been used for the activation of single neurons with high spatial-temporal resolution[8], even in motile animals[9], controlling cardiac function[10] and repairing vision[11].

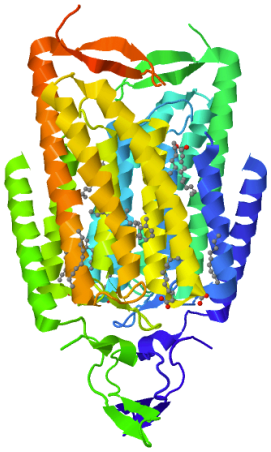

Figure 1-2. The structure of channelrhodopsin 2 (ChR2), a representative microbial opsin. It consists of homodimer. Wild-type ChR2 absorbs blue light with an absorption and action spectrum maximum at 480 nm. Most natural channelrhodopsins are nonspecific cation channels.

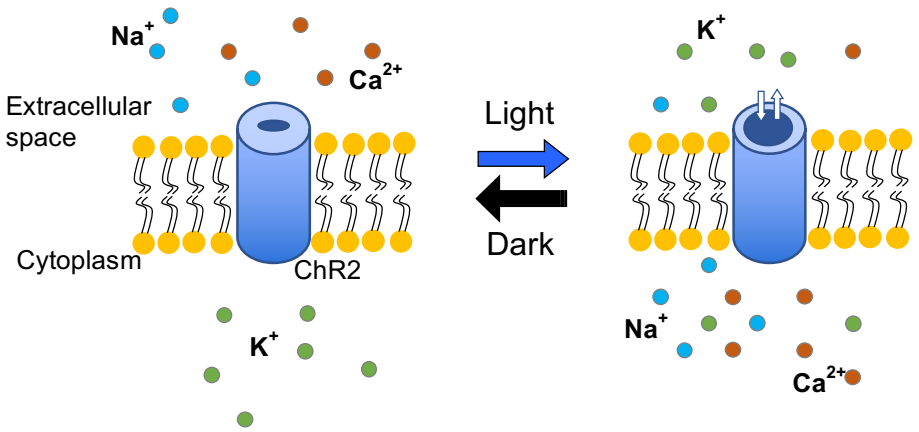

Figure 1-3. The behavior of channelrhodopsin 2 (ChR2). It uses retinal as its chromophore and induce ion fluxes in response to light. Most microbial channelrhodopsins (ChRs) are become permeable for cations when stimulated (maximum 480 nm), conducting H^+, Na^+, K^+, and Ca^{2+} ions nonspecifically.

The combination of halorhodopsins, chloride pumps driven by orange light, with channelrhodopsins (**Fig. 1-3**), opened by blue light, enabled neuronal activity to be switched on and off by using light-pulses of two different wavelengths[12,13]. Latterly, optogenetic systems have been extended even in control of cellular signaling and gene expression in bacteria[14–18], yeast[19–24] and mammalian cells[20,23–31]. Other light-sensitive targets involve molecules such as ion channels and receptors, and phenomena such as inducible protein-protein interactions, proteolysis and subcellular translocation of proteins. Moreover, controlling second messengers and cell morphology change with optogenetic systems have also been accomplished.

From here, I focus on the field of non-neuronal optogenetics whose potential for the generation of various applications in mammalian cells has just started to be realized within the last several years.

In the next section, along with **Table 1-1**, I describe the variety of different photoreceptors, such as light-oxygen-voltage (LOV) domains[32], cryptochrome[23,33] (CRY), phytochrome[27] (PHY), the fluorescent protein Dronpa[34] and UVR8[35,36]. They were applied to regulate particular events in mammalian cell signaling[37–41].

Table 1-1. Characterization of individual light-sensitive protein pairs in optogenetic toolboxes. Each size (length of amino acid sequence), harbored cofactors, used light wavelength upon association and dissociation, and time needed for association/dissociation from each binding partner are shown.

photoreceptor	Size (amino acids)	cofactor	Association/dissociation wavelength (nm)	Association /dissociation time	Refs
LOVpep/ePDZ	153/194	FMN	450/dark	s / 81 s	[24]
FKF1/GI	619/1173	FMN	450/dark	min / >100000 s	[26]
EL222	150	FMN	450/dark	s / 2.7 – 16000 s	[51]
VVD/VVD	150/150	FAD	450/dark	s / 18000 s	[50]
Magnet	150/150	FAD	450/dark	s / 5 – 17000 s	[76]
CRY2/CIB1	612/335	FAD	450/dark	s / 6 min	[23]
CRY2/CRY2	498/498	FAD	450/dark	s / 6 min	[45]
CRY2olig	498	FAD	450/dark	s / 23 min	[33]
PhyB/PIF6	908/100	PCB	650/750	s / s	[27]
Dronpa/Dronpa	257/257	None	390/490	s / s	[47]
UVR8/COP1	440/340	None	Dark/290-310	1-4h / s	[64]

I-II Overview of optogenetic systems

Photoreceptors, proteins that change conformation upon light exposure, have been employed to induce various cellular signaling. Five kinds of photoreceptors and their applications, that is, optogenetic systems, are introduced here. Three of these photoreceptors are based on photo-responsive proteins from plants (light-oxygen-voltage (LOV) domains[24,28,42,43], cryptochromes[23,44,45], and phytochromes[19,27,46]). Another is based on Dronpa[47], which is a fluorescent protein isolated from the coral *Pectiniidae*[48]. Lastly, UVR8[49] (Ultraviolet Response 8) from plant, *A. thaliana*.

I-II-(i) LOV domains

The LOV domains, including AsLOV2[42], FKF1[26], VVD[50], and EL222[51], have been used extensively as components of optogenetic systems. They are sensitive to blue light (440–473 nm) and harbor the endogenous flavin derivatives [FMN (flavin mononucleotide) or FAD (flavin adenine dinucleotide)] as chromophores (**Fig. 1-4**). They are abundant in cells; hence there is no necessity of addition of cofactors from outside the cells. Upon blue light (maximum 450 nm) absorption, chromophores in the LOV domain form a covalent bond with a

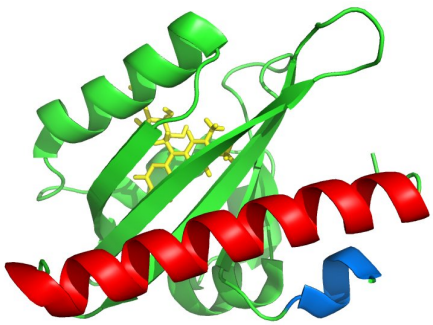

Figure 1-4. The structure of AsLOV2, representative of LOV domains. The red helix designates Jα helix. The blue helix, A'α helix. The yellow compound is a cofactor, FMN.

cysteine residue, which is located near the C-N aromatic bond of isoalloxazine ring of the cofactor[50]. Upon removal of the light, this reaction reverts within a few seconds to sometimes minutes by hydrolysis of the Carbon (of FMN)–cysteine bond, which is responsible for the interaction of LOV domains with their counterparts.

Each LOV system is different in respect of how the light-mediated conformational change induces a cellular signaling pathway. One method is to directly fuse an effector protein to the domain, and relieve the caging of the effector only when the conformation of the LOV domain changes upon light exposure[28]. In other LOV-based systems, the LOV domains heterodimerize with a natural or engineered counterpart to induce cellular signaling[24], as another LOV domain homodimerizes with each other and binds to specific sequences of DNA inside the nucleus, thereby inducing gene expression[30,51].

AsLOV2

AsLOV2 (LOV2 domain from *Avena sativa* phototropin 1) is the most commonly employed LOV protein for optogenetic systems. In this LOV2 domain, the FMN–cysteine covalent bond formation leads to partial unfolding of the C-terminal α-helix (Jα) from the rest of the PAS (Per-Arnt-Sim) core inside the LOV2 domain. This behavior was early applied to confer light sensitivity in an allosteric manner, in particular, on the dihydrofolate reductase (DHFR) by linking to a surface site and to a

transcription factor with the mutually independent folding of Jα and the N-terminal α-helix respectively[52,53]. Subsequently, AsLOV2 has been fused to the N-terminus of target domains or peptides to hide with steric blocks that are possible to be released by light-sensitive Jα unfolding (**Fig. 1-5**).

PA-Rac1

As an example of an application with AsLOV2, Wu et al.[28] tested several different linkages of AsLOV2 to the N-terminus of Rac1, one of Rho GTPases, and determined one that showed Rac1 response to blue light the best. The obtained construct, PA-Rac1 (photoactivable Rac1) (**Fig. 1-5**), enabled optical manipulation of cell membrane moving in mammalian cells.

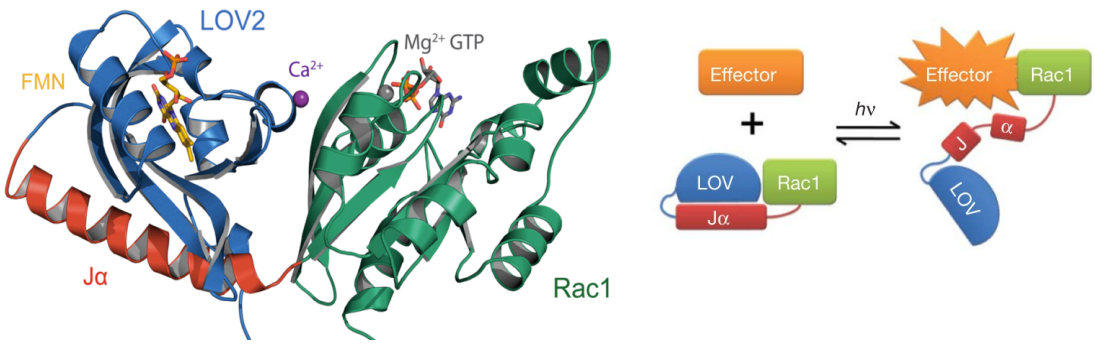

Figure 1-5. PA-Rac1. When the tool is exposed blue light, Jα unfolds, and steric hindrance on Rac1 is lost. Liberated Rac1 activates its effectors. In this way, the photo-induced activation of Rac1 is realized.

TULIP

Strickland et al.[24] created LOV2 fusions capable of light-mediated heterodimerization between a specific peptide fused to AsLOV2 and PDZ domains that bind the specific peptide. This system is named tunable light-controlled interacting protein tags (TULIPs) (**Fig. 1-6**). Irradiation of light induced peptide caging off and PDZ binding in yeast and mammalian cells, which is demonstrated by the translocation of PDZ fusion proteins to LOV2–peptide fusions located at the plasma membrane. They tested whether TULIP can be used for light-activated cellular signaling, including MAPK cascade (Ste5) and GTPase Cdc42.

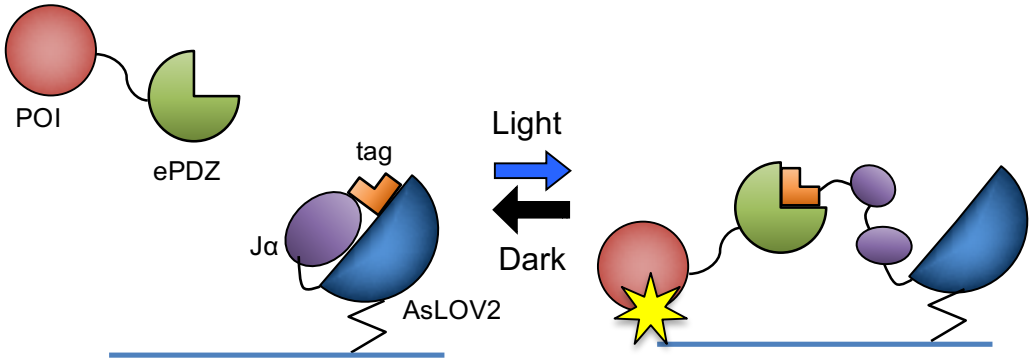

Figure 1-6. Schematic design of TULIPs. In the dark, a peptide epitope is caged by docking of the Jα helix to the LOV2 core (blue). Upon photoexcitation, the Jα helix undocks and exposes the peptide epitope tag, resulting in binding by ePDZ (green) and recruiting POI to the membrane where LOV2 is anchored.

iLID

Guntas et al.[54] fused the bacterial SsrA peptide to the C-terminal helix of the AsLOV2 domain. In the dark, the SsrA peptide is sterically blocked by the core of AsLOV2 from binding its natural binding partner, SspB. When irradiated with blue light, the Jα helix of the LOV2 domain undocks from the protein core, allowing the SsrA peptide to bind SspB (**Fig. 1-7**). Without optimization, the switch exhibited only a two-fold change in the binding affinity for SspB upon light exposure. They conducted computational protein design, phage display, and high-throughput binding assays to create an improved light-inducible dimer (iLID), which changes its affinity for SspB by over 50-fold upon light activation. The authors applied this new system to efficient induction of lamellipodia.

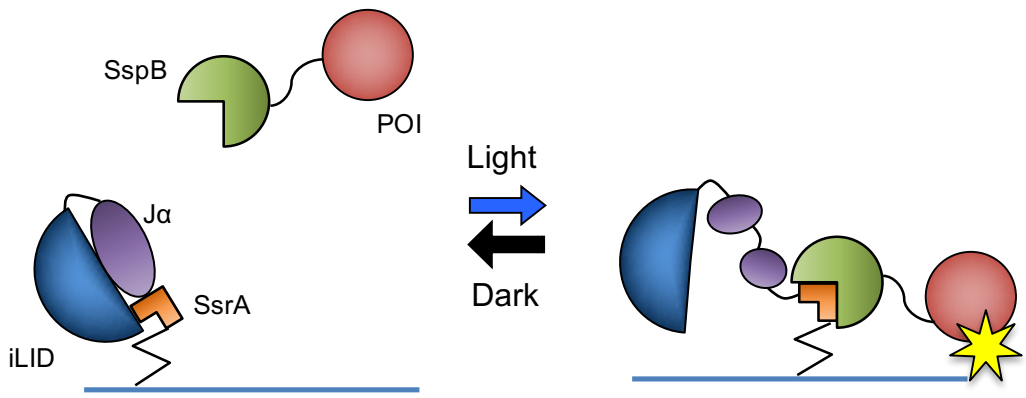

Figure 1-7. Schematic design of iLID. In the dark, a peptide is caged by docking of the Jα helix to the LOV2 core (blue). Upon photoexcitation, the Jα helix undocks and exposes the peptide SsrA, leading to binding with SspB. POI fused to SspB is translocated to the membrane where iLID is located.

FKF1/GI(GIGANTIA)

In plants, flavin-binding/Kelch-repeat/F-box 1 (FKF1), the FMN–cysteine bond formation leads to interaction between the FKF1 N-terminus and GI (GIGANTEA). Yazawa et al.[26] used this feature to translocate the proteins or its domains of interest to specific locations in mammalian cells upon light exposure. More specifically, they used light to translocate Rac1 fused to FKF1 to membrane anchors fused to GIs, enabling activation of endogenous membrane-bound Rac1 effectors (**Fig. 1-8**). Additionally, they similarly translocated a transcriptional activation domain fused with FKF1 to a DNA-binding domain fused with GI to activate transcription. This transcriptional regulation system using FKF1 and GI has been recently reproduced and enhanced by another group[31].

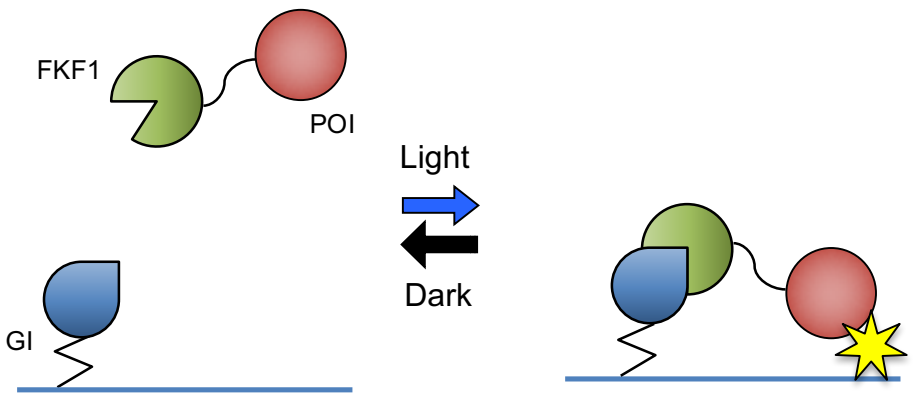

Figure 1-8. Schematic design of interaction of FKF1 and GI. Irradiated with blue light, FKF1 changes its conformation to be light-state, and binds GI. In this phenomenon, POI is translocated to the plasma membrane.

EL222

EL222 only consists of the minimal elements needed for light-dependent transcriptional activation: a photo-sensing LOV[55] domain and a helix-turn-helix (HTH) DNA-binding domain. In the dark, the LOV domain interacts with the HTH domain harboring 4α helix essential for dimerization and DNA binding[56]. Blue light irradiation (450 nm) triggers the photochemical reaction that results in formation of a protein-flavin adduct inside the LOV domain, which releases the inhibition of LOV-HTH interactions, enabling EL222 to dimerize and bind DNA[57,58].

Motta-Mena et al.[51] reported that an engineered variant of EL222 activated transcription in eukaryotic systems upon blue light stimulation (**Fig. 1-9**). They demonstrated over 200-fold improvement of gene expression from an EL222-responsive luciferase reporter in HEK 293T cells upon blue light irradiation without disturbing robust cellular growth. In contrast, In the dark or under red light exposure, the system showed changes less than two-fold response, establishing minimal leakage in non-inducing state. Their system showed fast activation (< 10 s) and deactivation (< 50 s) kinetics, which compares favorably to the < 2 h turn-off kinetics of a recently engineered LOV-based transcriptional system[30]. Also, they demonstrated that EL222 enabled either global or tissue-specific light-dependent gene expression in zebrafish without toxicity, expanding the utility of this expression system.

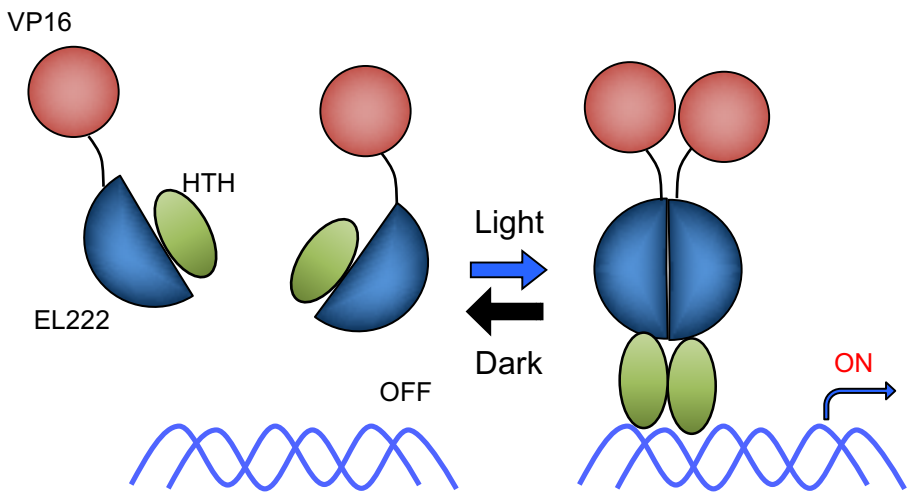

Figure 1-9. The transcription system (VP-EL222 protein) consists of the transcriptional activation domain from the VP16 protein fused to EL222. In the dark, VP-EL222 is unable to bind DNA. Exposure to blue light triggers a photochemical reaction between the LOV domain and its flavin chromophore, which activates the attached HTH domain to bind DNA and turn on gene transcription by recruited VP16.
HTH: helix-turn-helix.

(VVD)

Another LOV domain photoreceptor, VVD, is described in the later section.

I-II-(ii) Cryptochrome 2

Cryptochrome 2 (CRY2) is a protein from *Arabidopsis thaliana* that absorbs blue light (405–488 nm). When irradiated with blue light, CRY2 homo-oligomerizes[45] or binds to CIB1 (cryptochrome-interacting basic helix-loop-helix 1)[59] in seconds[23]. The presence of CIB1 induces heterodimerization, and in its absence, CRY2 molecules form large clusters. After approximately six minutes in the dark, the conformation of the activated CRY2 reverts to that before irradiation of blue light. CRY2 harbors FAD, which is abundant in mammalian cells, as its chromophore.

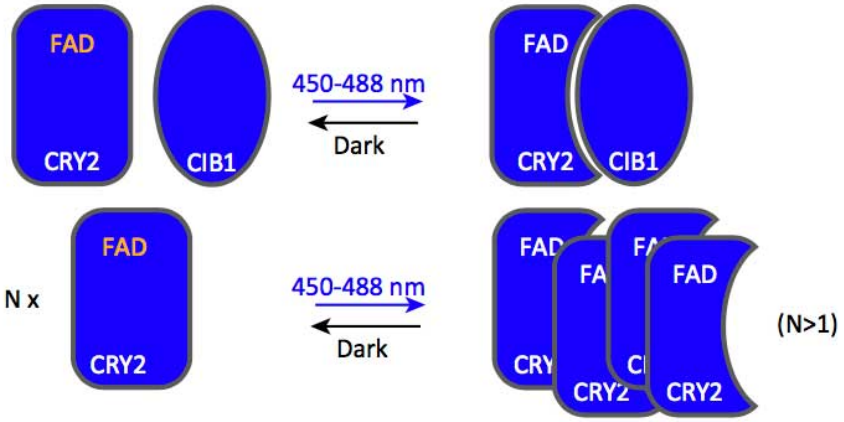

Figure 1-10. CRY2 behavior under the blue light. When exposed to blue light, CRY2 binds to CIB1 (up). In the absence of CIB1, CRY2 (CRY2olig) form large clusters (down).

CRY2/CIB1

Kennedy et al.[23] reported genetically encoded light-inducible protein-interaction systems based on CRY2 and CIB1 that need no exogenous compounds and dimerize upon blue light exposure with subsecond time resolution and subcellular spatial resolution (**Fig. 1-10**). They demonstrated the versatility of the

system by inducing protein translocation, transcription, and Cre recombinase–mediated DNA recombination with light.

CRY2olig

Taslimi et al.[33] described a new CRY2-based optogenetic system, 'CRY2olig', that enables detection of protein interactions in live cells, as well as perturbation of protein function with light. When stimulated by a pulse of light, CRY2olig undergoes rapid, reversible, and robust clustering within seconds (**Fig. 1-10**), gathering cytosolic proteins into clusters in every irradiated cell. Although wild-type CRY2 also clusters under certain conditions[45], clustering of CRY2olig is stunningly enhanced, enabling induction of cellular signaling. Moreover, CRY2olig is able to be used to evoke reversibly control diverse cellular processes with spatial and temporal resolution. Besides, they demonstrated querying protein-protein interactions, the disruption of clathrin-mediated endocytosis, and activation of Arp2/3-mediated actin polymerization with light.

CLICR

Bugaj et al.[60] reported a genetically encoded approach based on CRY2, termed Clustering Indirectly using Cryptochrome 2 (CLICR). This system is for spatiotemporal control over endogenous transmembrane receptor activation. This process is enabled through the optical manipulation of target receptor clustering and

downstream cellular signaling using non-covalent clustering with engineered CRY2s. Through photo-responsive multimerization of CRY2s, powerful induction of cellular signaling was accomplished (**Fig. 1-11**). CLICR offers a modular platform to enable optical manipulation of the clustering of different transmembrane receptors including fibroblast growth factor receptor (FGFR), platelet-derived growth factor receptor (PDGFR), and integrins in various cell types such as neural stem cells. Also, light-inducible control of endogenous receptor tyrosine kinase (RTK) activity can modulate cell polarity and establish phototaxis in fibroblasts. The disadvantage of this system is that the number of CRY2 molecules is uncontrollable, thereby multimers form aggregation that might inhibit the behavior of the system.

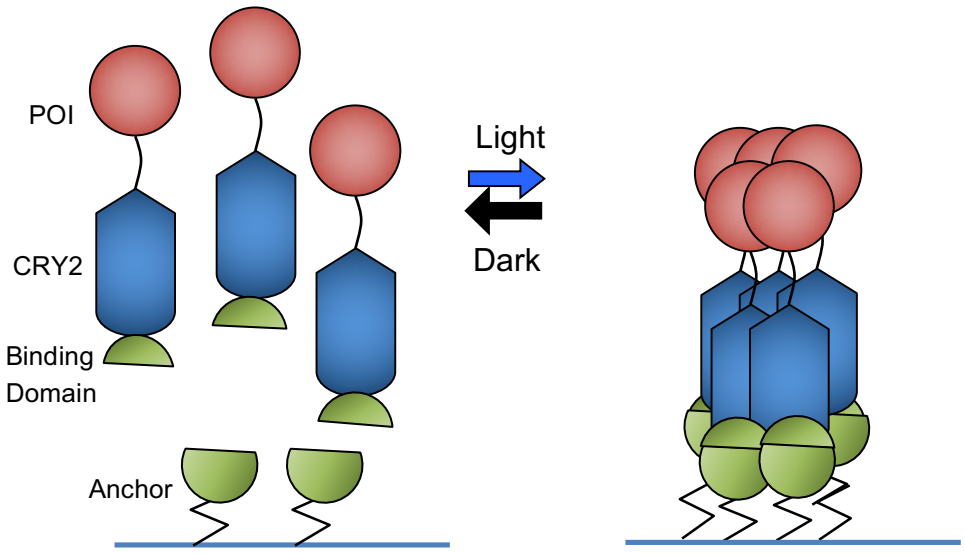

Figure 1-11. CLICR allows modular Cry2 clustering and activation of membrane receptors via noncovalent interactions, avoiding complications associated with overexpression of receptor fusions. With CLICR, Cry2 fused to a receptor-targeting binding domain (BD) is expressed in the cytoplasm. In the dark, unclustered state, BD affinity for the receptor is weak and imparts no or little membrane localization. On light-induced clustering, BD-Cry2 oligomers increase local BD concentration, enabling membrane translocation, binding and nucleation of a receptor cluster.

I-II-(iii) Phytochrome

Phytochrome (Phy) is a protein that normally regulates seedling stem elongation in *A. thaliana.* Irradiated by infrared light (740 nm) (**Fig. 1-12**). Upon expression, apo-Phy (not bound to a chromophore) spontaneously absorbs phycocyanobilin (PCB), a chromophore found in photosynthetic organisms, and becomes red light-responsive; however, in organisms that do not perform photosynthesis, PCB must be introduced into cells artificially or synthesized by exogenous enzymes[61,62]. Upon red light (660 nm) exposure, PCB-bound Phy (holo-Phy) changes its conformation to Pfr form, active state, and interacts with phytochrome interacting factor (PIF)[46] within seconds. This interaction is stable for hours in the dark, but can be reverted (Pr form, inactive state) within seconds by infrared light exposure[27].

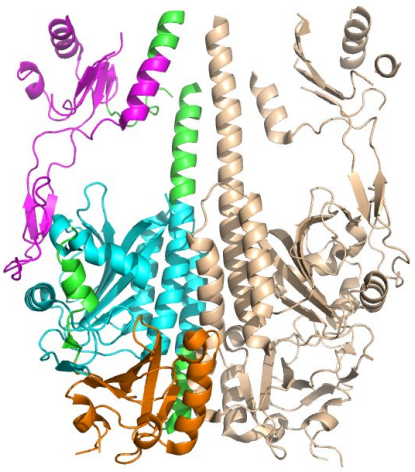

Figure 1-12. The structure of photosensing module of plant (*Arabidopsis thaliana*) PhyB in Pr (inactive) state.

Shimizu-Sato et al.[19] demonstrated that the light-dependent interaction of PhyA with PIF3 enable to control transcription in yeast cells added with phycocyanobilin. Light-induced recruitment of a transcriptional activation factor fused with PIF3 to a DNA-binding domain fused with PhyA increased in gene transcription. Levskaya et al.[27] showed the PhyB–PIF6 interaction can control translocation of the Rac activator

Tiam to the membrane in mammalian cells added with phycocyanobilin (**Fig. 1-13**). Local irradiation resulted in the local lamellipodia formation, as expected with Rac activation. The absorption of red light by Phys contrasts with the blue light absorption by flavin-binding proteins. Red light would be desirable for the lower photo-toxicity and improved penetration through tissue. However, this system has shown slower introduction by cell biologists than the LOV domain or cryptochrome-based systems. Reasons for the reduced number of applications using Phy–PIF system could be the necessity to tediously adding with the chromophore, the high sensitivity of Phy domains and a requirement for high Phy expression levels[63].

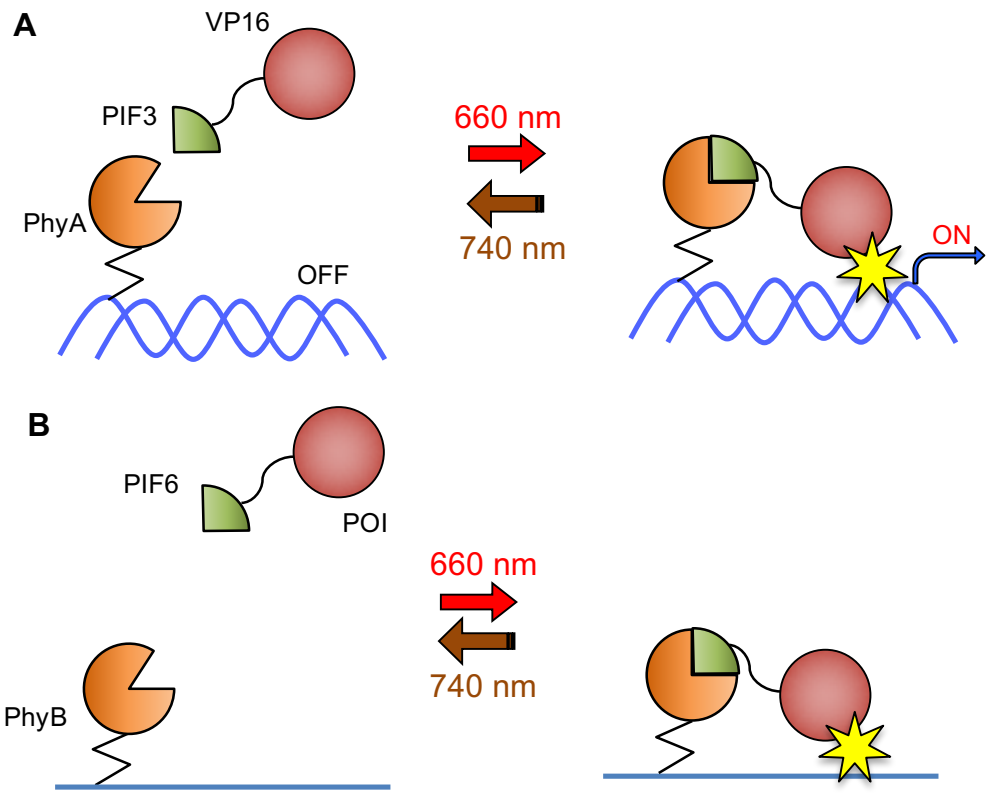

Figure 1-13. Light-induced heterodimerization between phytochrome and PIF has been used to upregulate transcription (A) and to control protein localization (B). The chromophore of phytochrome is phytochromobilin. POI; Protein of interest.

I-II-(iv) Dronpa

Dronpa is a fluorescent protein (FP) that is activated by light (photoactivatable FP). Photoactivation not only changes the fluorescence of FP but also modifies its quaternary structure. In the dark state (not photoactivated), Dronpa is a monomer; in the activated state, it forms a dimer (**Fig. 1-14**). The Dronpa-based system was found to be more robust when the protein system is in the dimeric state. On the other hand, in monomer state, Dronpa has a low affinity for each other; therefore, to facilitate dimerization, each copy of Dronpa is fused respectively to the amino and carboxyl termini of a protein of interest (POI). When the system is irradiated with UV light at 390 nm, the Dronpa domains at both ends of POI bind to each other; this binding inhibits the function of the POI by changing the conformation of POI with the steric hindrance of Dronpa dimer. The extent of protein inhibition can be traced by the change in the intensity of fluorescence of Dronpa. This inhibition can be reversed by irradiation with blue light at 490 nm, which reverts Dronpa back to a monomer[47], and the POI recovers activity (**Fig. 1-15**). Dronpa has an internal chromophore; hence there is no need for adding chromophore to the system. Latterly, Dronpa was further engineered to change

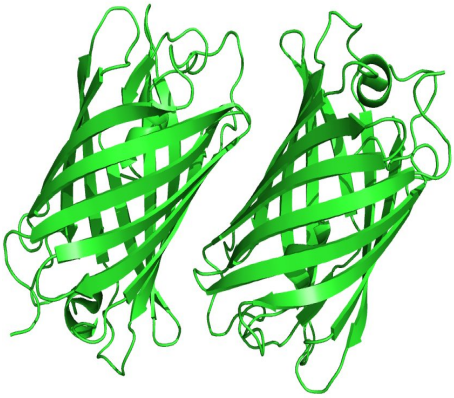

Figure 1-14. The structure of Dronpa dark-state dimer. When exoposed to the UV light, they associate to be homodimers.

its oligomeric state by activation. By introduction of the K145N substitution, a homotetrameric complex was formed, monomerizing through irradiation with blue light (**Fig. 1-16**). Dronpa was successfully applied by Zhou et al. for photo-caging of enzymes and mediators of cellular signaling and membrane translocation (fluorescent protein mNeptune)[47].

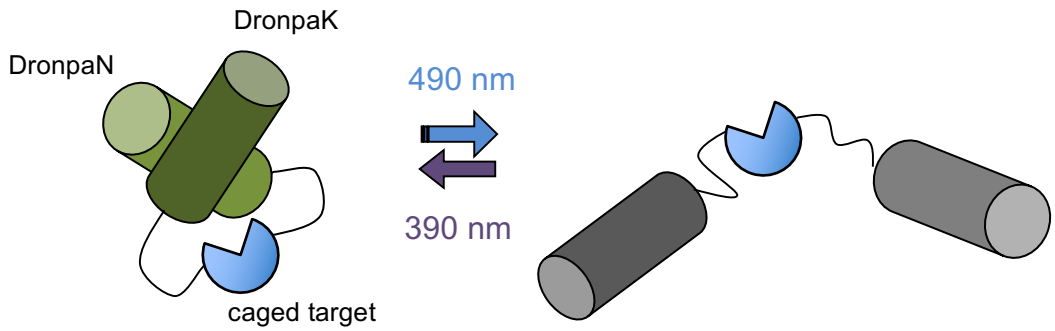

Figure 1-15. Light-induced heterodimerization between DronpaK and DronpaN can be utilized to cage targets such as GEFs, activated by violet light, and inactivated by blue light respectively. DronpaN is mutant with K145N substitution.

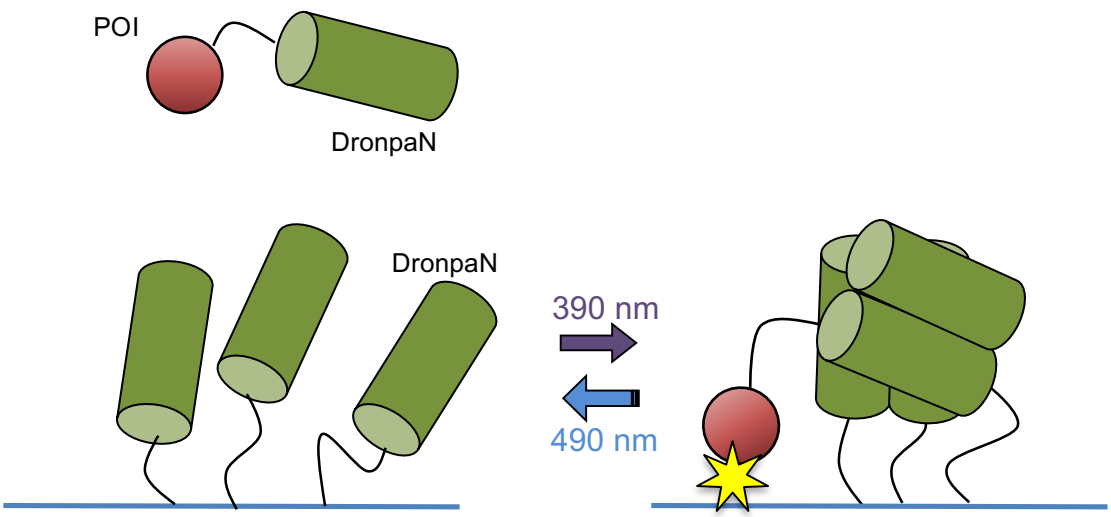

Figure 1-16. The POI can be recruited to plasma membrane anchored DronpaN in a tetrameric complex when fused to DronpaN. The recruitment with 490 nm light is reversed upon illumination with 390 nm light.

I-II-(v) UVR8 (ULTRAVIOLET RESPONSE 8)

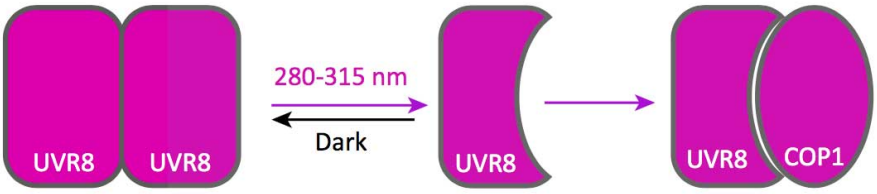

Figure 1-17. UVR8 forms homodimers in the dark. They dissociate upon UV illumination, after which the monomers are able to bind COP1.

A couple of years ago, a plant protein had been characterized that demonstrated light-manipulated binding without using any cofactors. UVR8 forms homodimers that dissociate upon UV irradiation, and the monomers can bind CONSTITUTIVELY MORPHOGENIC 1 (COP1)[64,65] (**Fig. 1-17**). The natural chromophores in UVR8 are a pair of tryptophan residues (aromatic π-bonds) that are involved in cation–π interactions with arginine residues (cation) at the dimeric interface. It is speculated that photon absorption effects breakage of the cation–π interactions, yielding subtle conformational changes that next break the hydrogen-bonds at the dimeric interface[64,65]. The conformational change is significantly long-lived, persisting many hours.

UVR8 and COP1 were used by two groups to control protein heterodimerization in mammalian cells with UV light. Muller et al.[66] fused UVR8 to a DNA-binding domain and COP1 to a transcriptional activation factor (**Fig. 1-18**), as Crefcoeur et al.[35] reversed the sequential order of UVR8 and COP1 and regulated the subcellular localization of POI (**Fig. 1-19**). However, the disadvantage of the UVR8–

COP1 system is that it requires prolonged exposure to UV light that is mutagenic and phototoxic, although acute phototoxicity can be minimized by applying UV light pulses[35,66].

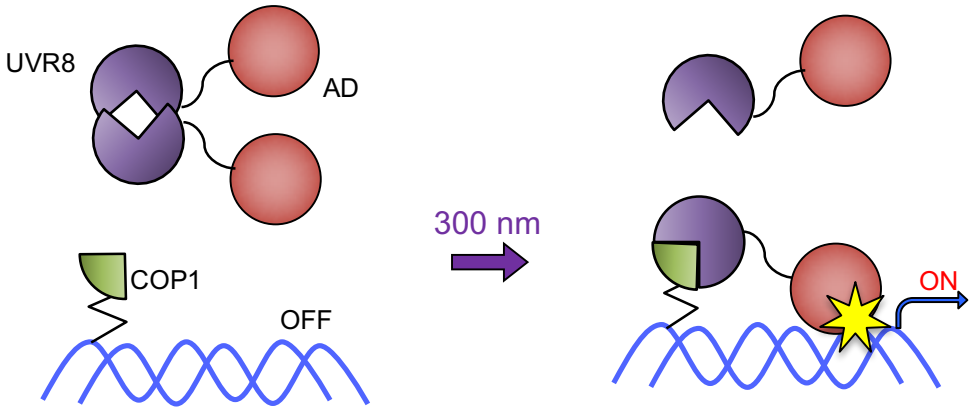

Figure 1-18. Light induced heterodimerization by UVR8 has been used to control transcription. In the dark, UVR8 forms homodimer. Irradiated UV light, UVR8 dissociates to be monomer and bind to COP1.

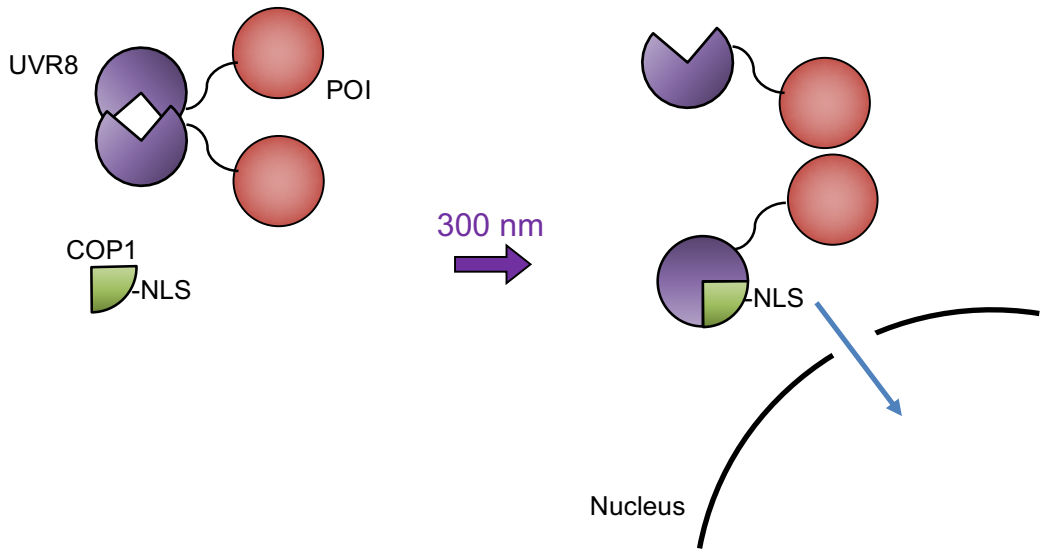

Figure 1-19. Light induced heterodimerization by UVR8 has been used to control protein localization, in this case, cytoplasm-to-nucleus transport of POI. In the dark, UVR8 forms homodimer. Irradiated UV light, UVR8 dissociates to be monomer and bind to COP1.

I-III Photoreceptor Vivid (VVD)

VVD is a LOV protein, isolated from *Neurospora crassa*, involved in the adaptation to increasing levels of blue light[67,68] (**Fig. 1-20**). VVD has only a photosensitive LOV domain connected to an Ncap (a long and flexible peptide domain at the amino-termini of VVD) needed for cellular signal transduction by stabilizing homodimerization[50]. In contrast to AsLOV2, another LOV domain that has Jα helix, cellular signaling evoked by VVD does not need an effector domain, but involves the light-dependent homodimerization of VVD[69]. Structurally, VVD is one of only two LOV proteins that have had the crystal structure obtained for both the dark and light states, offering valuable insights into the mechanism of signal transduction by LOV proteins.

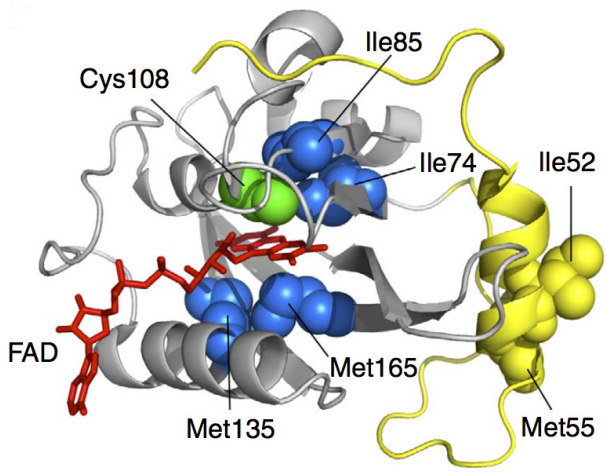

Figure 1-20. Crystal structure of VVD in the dark state, and important residues interacting with the cofactor FAD. Cys108 makes the covalent bond with FAD when irradiated with blue light. Ile74 has van der Waals contact with Cys108. Met135 and Met165 supports the isoalloxazine ring. Ile52 and Met55 make interaction surface of dimerization.

The crystal structures indicated a mechanism of emitting cellular signal similar to that of AsLOV2, but with a different functional outcome. Structural data reveal that the apparent rotation of Q182 occurs following a combination of C4a adduct formation and N5 protonation[43] (**Fig. 1-21**). Rotation of Q182 favors the formation of H-bonds with the newly protonated N5 of the chromophore FAD and the resulting changes in the H-bond network spread to the surface of the protein through interactions with A72 within Aβ (**Fig. 1-22**). These lead to changes in the Ncap structure through a common hinge region[43,70–73]. The key point of signal propagation is C71, which resides at a deep position, and its rotation generates a large change in the positional relationship between the LOV core and Ncap. Hydrophobic clefts exposed by these movements support homodimerization mediated by the modified Ncap structure. Small-angle X-ray scattering (SAXS) and light-state crystal structures indicate that VVD is a low-affinity, rapidly exchanging dimer under the influence of the reorganization of Ncap.

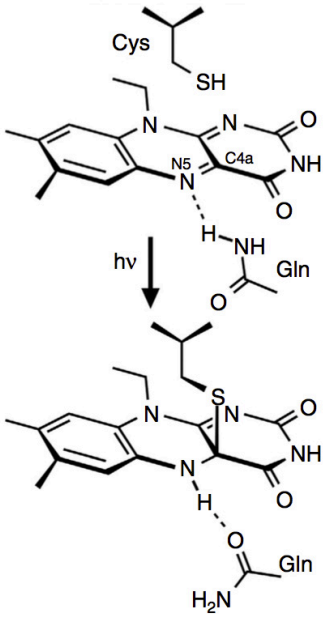

Figure 1-21. Signal propagation in VVD is initiated by a combination of C4a adduct formation with the cysteine of AsLOV2 and N5 protonation on isoalloxazine ring of FAD. Protonation of the N5 position alters H-bonding contacts to a glutamine residue.

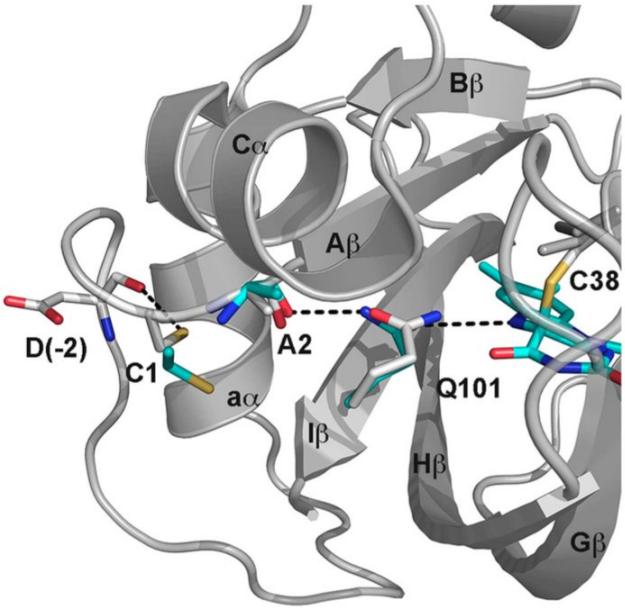

Figure 1-22. VVD signaling. Each residue number designate Q182 (Q101), C108 (C38), A72 (A2), C71 (C1) and D68 (D-2). These residues propagate the changes of hydrogen bonds network that starts at Q182 to the Ncap when irradiated with blue light. C4a adduct formation promotes rotation of Q182 to change H-bonds to A72. Displacement of the Ncap reorientates C71 to disrupt contacts with D-2, providing rearrangement of the Ncap and dimer formation.

LightOn system

Wang et al.[30] developed a light-switchable transgene system based on VVD and a synthetic, genetically encoded light-switchable transactivator (**Fig. 1-23**). The transactivator interactions the promoter when irradiated with blue light and quickly initiates transcription of target genes in mammalian cells and in mice. They named the gene promoter system based on VVD 'LightOn'.

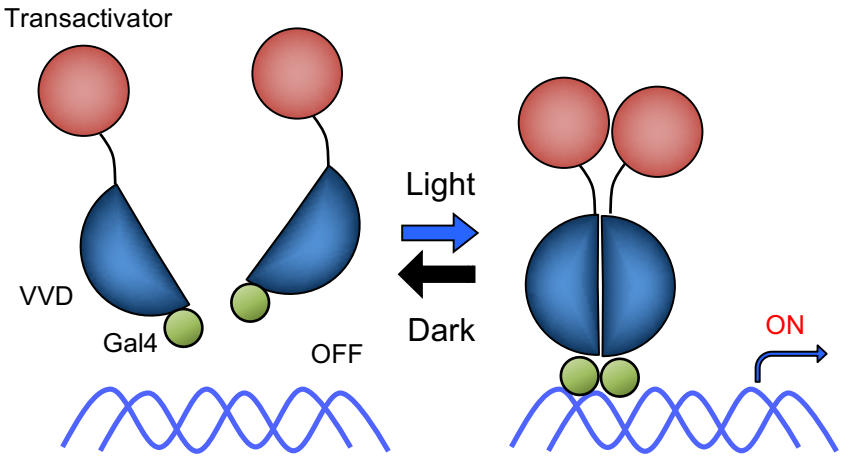

Figure 1-23. Schematic representation of the LightOn system. After light activation, VVD with Gal4 homodimerizes, interacts with correspondent elements and initiates expression of the gene of interest.

Light-dependent dimerization makes VVD an ideal candidate optogenetic tool for regulating protein interactions; however, the low dimer affinity and long-lasting active state limit its versatility. Some novel approaches have been used to both harness and improve VVD as an optogenetic tool. One of those approaches is the VVD LightOn system, described above, which is a modification of yeast and mammalian 2-hybrid approaches[74,75]. In the next section, I will focus on the 'Magnet system' engineered in our laboratory to highlight the structural and chemical tuning of VVD.

I-IV Magnet system

The VVD-based magnet system focused on rectifying two limitations of VVD-based tools, that is, slow on and off kinetics and low dimer affinity. The magnet system modified the Ncap structure, which was key for developing a pair of VVD variants that can only heterodimerize and do not form homodimers. Specifically, we introduced charged residues into strategic regions of the interacting surfaces of VVD (Ile52 and Met55). By creating a modified VVD pair, one with a negative charge (Arg52/Arg55) and another with a positive charge (Asp52/Gly55), we were able to achieve a robust system with ~40-fold activation upon light irradiation[76]. By introducing a slow-cycling variant with higher affinity in one component, paired with a fast-cycling mutant in the other, we achieved further amplification of the signal output and improved the on/off kinetics. The newly engineered system offers modifiable kinetics (four orders of magnitude) and signal strength (a maximum of a 13-fold increase in signal intensity)[76]. The magnet system enabled me to manipulate cellular processes such as protein-protein interactions[76] (**Fig. 1-24**) and genome editing[77].

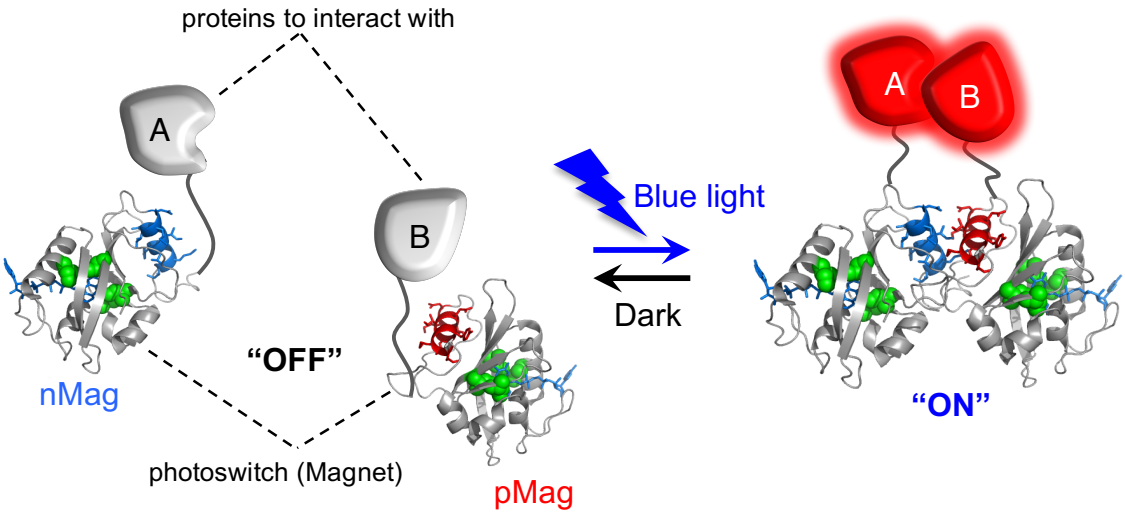

Figure 1-24. The Magnet system. The blue-light dependent dimerization assists the complementation of fused protein to each other magnet. Upon the blue-light exposure, complemented fragments of protein acquire the activity. In the dark, Magnet dissociates from each other, and the fragments of protein lose the activity.

One of the magnet variants, pMagFast2 (**Table 1-2**), showed a rapid off rate (the rate of dissociation from nMagFast2, 25 s[76]) and has the potential to produce a highly functional optogenetic system. However, there were several aspects of the system that could still be improved upon. For example, although pMagFast2 is a fast kinetics version of pMag, its binding affinity is lower than normal pMag. In the present study, I aimed to resolve the problems within the magnet system and develop a new, highly functional optogenetic tool based on the magnet system, with a quick off-rate and exquisite spatiotemporal specificity. An optogenetic system based on this photoswitch, the enhanced magnet system, showed highly efficient induction of cellular functions with precise spatiotemporal controllability.

Table 1-2. The variants of Magnets. "$t_{1/2}$" indicates half-life of dissociation from each other magnet. For example, interaction between pMagHigh1 and nMagHigh1 lasts for 4.7 hours. High1 shows best affinity, but it takes a lot of time for them to dissociate from each other. On the other hand, Fast2 dissociates from the partner in seconds. Ref [76]. WT; wild type.

Magnets	mutation	$t_{1/2}$
VVD (WT)	Ile52, Met55	
pMag	Arg52, Arg55	
nMag	Asp52, Gly55	
MagHigh1	Ile74, Ile85, Ile135, Ile165	4.7 h
Mag(Normal)	Ile74, Ile85, Met135, Met165	1.8 h
MagFast1	Ile74, Val85, Met135, Met165	4.2 min
MagFast2	Val74, Val85, Met135, Met165	25 s

I-V Purpose of the present study

The dissociation kinetics of the Magnet system described above is faster than that of any other optogenetic tool (**Table 1-3**). I attempted to utilize this advantage to create a new system with high avidity and spatiotemporality. To evaluate the efficiency and spatial-temporal fidelity of the optogenetic systems, I used photo-induced translocation to plasma membrane and formation of lamellipodia.

In Chapter 2, I focused on the drawbacks of the Magnet system and strategies for its improvement. Although the Magnet system possesses many advantages including fast kinetics, low background activity and small size, its drawback is the low affinity between pMag and nMag. In the previous study, the lack of affinity was resolved, but another problem, the low expression of the system, arose. Therefore, I introduced a self-assembly domain into the Magnet system, which overcame the drawback and conferred high avidity to the system simultaneously.

In Chapter 3, I discuss application of the improved system to photo-manipulation of cellular signaling by fusing functional domains to CAD-Magnet. CAD-Magnet system has high avidity as verified in Chapter 2 and is able to hold many functional domains in an assembled probe at the same time. Under this working hypothesis, I compared the efficiency of inducing the plasma membrane response between the CAD-Magnet and tandemly-repeated Magnet to show the superiority of the power of CAD-Magnet. I successfully induced the plasma membrane morphology

changes at the place and the time of interest with light, and the CAD-Magnet system was more efficient. I affirmed that this improved Magnet system shows large-scale membrane ruffle and lamellipodia. In addition, I created a 4D movie of photo-regulation of the new Magnet system with the functional domains. This is a new attempt by high-speed scanning confocal florescence microscopy with high spatial-temporal resolution. Previous studies of optogenetic regulation mainly focused on the edge of the plasma membrane by 2D movie, but I have also analyzed intracellular surface of the plasma membrane (apical ruffle) using 3D live scanning.

Table 1-3. Summary of application of individual light-sensitive protein pairs in optogenetic toolboxes. In "Membrane recruitement", "Dissociation times" are shown. These indicate times needed for dissociation from plasma membrane in the dark. '– (inducible)' indicates that the system dissociates from membrane upon light exposure. HTH; helix-turn-helix.

Application	System	Signaling targets	Dissociation time	Refs
Membrane recruitment	pa-Rac	Rac1	43 s	[28]
	iLID	Tiam1	< 30 s	[54]
	FKF1/GI	Rac1	> 100000 s	[26]
	PhyB/PIF6	Tiam1	– (inducible)	[27]
	Dronpa	mNeptune	– (inducible)	[47]
	Magnet	PI3K, Tiam1	< 10 – 17000 s	[76]
Gene Expression	EL222	HTH	< 50 s	[51]
	VVD	Gal4	< 7200 s	[30]
	CRY2/CIB1	Gal4	ND	[23]
	UVR8/COP1	VP16	7100 s	[66]
Protein caging	Dronpa	Cdc42	– (inducible)	[47]
Protein inactivation	CRY2, MD	Vav2	340 s	[78]

I-VI References

1. Inoue, T., Heo, W. Do, Grimley, J. S., Wandless, T. J. & Meyer, T. An inducible translocation strategy to rapidly activate and inhibit small GTPase signaling pathways. *Nat. Methods* **2,** 415–418 (2005).
2. Deisseroth, K. Optogenetics. *Nat. Methods* **8,** 26–29 (2011).
3. Gardner, L. & Deiters, A. Light-Controlled Synthetic Gene Circuits. *Curr. Opin. Chem. Biol.* **16,** 292–299 (2012).
4. Rein, M. L. & Deussing, J. M. The optogenetic (r) evolution. *Mol.Genet.Genomics* **287,** 95–109 (2012).
5. Fenno, L., Yizhar, O. & Deisseroth, K. The Development and Application of Optogenetics. *Annu. Rev. Neurosci.* **34,** 389–412 (2011).
6. Blaurock, A. E., Stoeckenius, W., Oesterhelt, D. & Scherphof, G. L. Structure of the cell envelope of Halobacterium Halobium. *J. Cell Biol.* **71,** 1–22 (1976).
7. Melyan, Z., Tarttelin, E. E., Bellingham, J., Lucas, R. J. & Hankins, M. W. Addition of human melanopsin renders mammalian cells photoresponsive. *Nature* **433,** 741–745 (2005).
8. Boyden, E. S., Zhang, F., Bamberg, E., Nagel, G. & Deisseroth, K. Millisecond-timescale , genetically targeted optical control of neural activity. **8,** 1263–1268 (2005).

9. Tsai, H.-C. *et al.* Phasic Firing in Dopaminergic Neurons Is Sufficient for Behavioral Conditioning. *Science* **324,** 1080–1084 (2009).

10. Bruegmann, T. *et al.* Optogenetic control of heart muscle in vitro and in vivo. *Nat. Methods* **7,** 897–900 (2010).

11. Doroudchi, M. M. *et al.* Virally delivered Channelrhodopsin-2 Safely and Effectively Restores Visual Function in Multiple Mouse Models of Blindness. *Mol. Ther.* **19,** 1220–1229 (2011).

12. Zhang, F. *et al.* Multimodal fast optical interrogation of neural circuitry. *Nature* **446,** 633–639 (2007).

13. Kleinlogel, S. *et al.* A gene-fusion strategy for stoichiometric and co-localized expression of light-gated membrane proteins. *Nat. Methods* **8,** 1083–1088 (2011).

14. Levskaya, A. *et al.* Engineering Escherichia coli to see light. *Nature* **438,** 441–442 (2005).

15. Tabor, J. J. *et al.* A Synthetic Genetic Edge Detection Program. *Cell* **137,** 1272–1281 (2009).

16. Tabor, J. J., Levskaya, A. & Voigt, C. A. Multichromatic control of gene expression in Escherichia coli. *J. Mol. Biol.* **405,** 315–324 (2011).

17. Möglich, A., Ayers, R. A. & Moffat, K. Design and Signaling Mechanism of Light-Regulated Histidine Kinases. *J. Mol. Biol.* **385,** 1433–1444 (2009).

18. Ohlendorf, R., Vidavski, R. R., Eldar, A., Moffat, K. & Möglich, A. From Dusk till

Dawn : One-Plasmid Systems for Light-Regulated Gene Expression. *J. Mol. Biol.* **416,** 534–542 (2012).

19. Shimizu-Sato, S., Huq, E., Tepperman, J. M. & Quail, P. H. A light-switchable gene promoter system. *Nat. Biotechnol.* **20,** 1041–4 (2002).

20. Bulina, M. E. *et al.* A genetically encoded photosensitizer. *Nat. Biotechnol.* **24,** 95–99 (2006).

21. Tyszkiewicz, A. B. & Muir, T. W. Activation of protein splicing with light in yeast. *Nat. Methods* **5,** 303–305 (2008).

22. Sorokina, O. *et al.* A switchable light-input, light-output system modelled and constructed in yeast. *J. Biol. Eng.* **3,** 15 (2009).

23. Kennedy, M. J. *et al.* Rapid blue-light-mediated induction of protein interactions in living cells. *Nat. Methods* **7,** 973–975 (2010).

24. Strickland, D. *et al.* TULIPs : tunable , light-controlled interacting protein tags for cell biology. *Nat. Methods* **9,** 379–384 (2012).

25. Schroder-Lang, S. *et al.* Fast manipulation of cellular cAMP level by light in vivo. *Nat. Methods* **4,** 39–42 (2007).

26. Yazawa, M., Sadaghiani, A. M., Hsueh, B. & Dolmetsch, R. E. Induction of protein-protein interactions in live cells using light. *Nat. Biotechnol.* **27,** 941–945 (2009).

27. Levskaya, A., Weiner, O. D., Lim, W. A. & Voigt, C. A. Spatiotemporal control of

cell signalling using a light-switchable protein interaction. *Nature* **461,** 997–1001 (2009).

28. Wu, Y. I. *et al.* A genetically encoded photoactivatable Rac controls the motility of living cells. *Nature* **461,** 104–108 (2009).

29. Ye, H., Daoud-El Baba, M., Peng, R.-W. & Fussenegger, M. A synthetic optogenetic transcription device enhances blood-glucose homeostasis in mice. *Science* **332,** 1565–1568 (2011).

30. Wang, X., Chen, X. & Yang, Y. Spatiotemporal control of gene expression by a light-switchable transgene system. *Nat. Methods* **9,** 266–269 (2012).

31. Polstein, L. R. & Gersbach, C. A. Light-Inducible Spatiotemporal Control of Gene Activation by Customizable Zinc Finger Transcription Factors. *J. Am. Chem. Soc.* **134,** 16480–16483 (2012).

32. Pudasaini, A., El-Arab, K. K. & Zoltowski, B. D. LOV-based optogenetic devices: light-driven modules to impart photoregulated control of cellular signaling. *Front. Mol. Biosci.* **2,** 1–15 (2015).

33. Taslimi, A. *et al.* An optimized optogenetic clustering tool for probing protein interaction and function. *Nat. Commun.* **5,** 4925 (2014).

34. Habuchi, S. *et al.* Reversible single-molecule photoswitching in the GFP-like fluorescent protein Dronpa. *Proc. Natl. Acad. Sci. USA* **102,** 9511–9516 (2005).

35. Crefcoeur, R. P., Yin, R., Ulm, R. & Halazonetis, T. D. Ultraviolet-B-mediated

induction of protein–protein interactions in mammalian cells. *Nat. Commun.* **4,** 1779 (2013).

36. Chen, D., Gibson, E. S. & Kennedy, M. J. A light-triggered protein secretion system. *J. Cell Biol.* **201,** 631–640 (2013).

37. Shcherbakova, D. M., Shemetov, A. a., Kaberniuk, A. a. & Verkhusha, V. V. Natural Photoreceptors as a Source of Fluorescent Proteins, Biosensors, and Optogenetic Tools. *Annu. Rev. Biochem.* **84,** 519–550 (2015).

38. Mueller, K. & Weber, W. Optogenetic tools for mammalian systems. *Mol. Biosyst.* **9,** 596–608 (2013).

39. Pathak, G. P., Vrana, J. D. & Tucker, C. L. Optogenetic control of cell function using engineered photoreceptors. *Biol. Cell* **105,** 59–72 (2013).

40. Möglich, A. & Moffat, K. Engineered photoreceptors as novel optogenetic tools. *Photochem. Photobiol. Sci.* **9,** 1286–1300 (2010).

41. Beyer, H. M., Naumann, S., Weber, W. & Radziwill, G. Optogenetic control of signaling in mammalian cells. *Biotechnol. J.* 1–11 (2014). doi:10.1002/biot.201400077

42. Christie, J. M., Salomon, M., Nozue, K., Wada, M. & Briggs, W. R. LOV (light, oxygen, or voltage) domains of the blue-light photoreceptor phototropin (nph1): Binding sites for the chromophore flavin mononucleotide. *Proc. Natl. Acad. Sci.* **96,** 8779–8783 (1999).

43. Harper, S. M., Neil, L. C. & Gardner, K. H. Structural basis of a phototropin light switch. *Science* **301,** 1541–1544 (2003).

44. Liu, H. *et al.* Photoexcited CRY2 Interacts with CIB1 to Regulate Transcription and Floral Initiation in Arabidopsis. *Science* **322,** 1535–1539 (2008).

45. Bugaj, L. J., Choksi, A. T., Mesuda, C. K., Kane, R. S. & Schaffer, D. V. Optogenetic protein clustering and signaling activation in mammalian cells. *Nat. Methods* **10,** 249–52 (2013).

46. Ni, M., Tepperman, J. M. & Quail, P. H. Binding of phytochrome B to its nuclear signalling partner PIF3 is reversibly induced by light. *Nature* **400,** 781–784 (1999).

47. Zhou, X. X., Chung, H. K., Lam, A. J. & Lin, M. Z. Optical control of protein activity by fluorescent protein domains. *Science* **338,** 810–4 (2012).

48. Ando, R. Regulated Fast Nucleocytoplasmic Shuttling Observed by Reversible Protein Highlighting. *Science* **306,** 1370–1373 (2004).

49. Christie, J. M. *et al.* Plant UVR8 Photoreceptor Senses UV-B by Tryptophan-Mediated Disruption of Cross-Dimer Salt Bridges. *Science* **335,** 1492–1496 (2012).

50. Zoltowski, B. D. *et al.* Conformational Switching in the Fungal Light Sensor Vivid. *Science* **316,** 1054–1057 (2007).

51. Motta-mena, L. B. *et al.* An optogenetic gene expression system with rapid

activation and deactivation kinetics. *Nat. Chem. Biol.* **10,** 196–202 (2014).

52. Lee, J. *et al.* Surface Sites for Engineering Allosteric Control in Proteins. *Science* **322,** 438–442 (2008).

53. Strickland, D., Moffat, K. & Sosnick, T. R. Light-activated DNA binding in a designed allosteric protein. *Proc. Natl. Acad. Sci. U.S.A.* **105,** 10709–10714 (2008).

54. Guntas, G. *et al.* Engineering an improved light-induced dimer (iLID) for controlling the localization and activity of signaling proteins. *Proc. Natl. Acad. Sci.* **112,** 112–117 (2015).

55. Huala, E. *et al.* Arabidopsis NPH1 : A Protein Kinase with a Putative Redox-Sensing Domain. *Science* **278,** 2120–2123 (1997).

56. Nash, A. I. *et al.* Structural basis of photosensitivity in a bacterial DNA-binding protein. *Proc. Natl. Acad. Sci. USA* **108,** 9449–9454 (2011).

57. Rivera-Cancel, G., Motta-Mena, L. B. & Gardner, K. H. Identification of natural and artificial DNA substrates for light-activated LOV-HTH transcription factor EL222. *Biochemistry* **51,** 10024–10034 (2012).

58. Zoltowski, B. D., Motta-Mena, L. B. & Gardner, K. H. Blue-light induced dimerization of a bacterial LOV-HTH DNA-binding protein. *Biochemistry* **52,** 6653–6661 (2013).

59. Mas, P., Devlin, P. F., Panda, S. & Kay, S. A. Functional interaction of

phytochrome B and cryptochrome 2. *Nature* **408,** 207–211 (2000).

60. Bugaj, L. J. *et al.* Regulation of endogenous transmembrane receptors through optogenetic Cry2 clustering. *Nat. Commun.* **6,** 7898 (2015).

61. Gambetta, G. A. & Lagarias, J. C. Genetic engineering of phytochrome biosynthesis in bacteria. *Proc. Natl. Acad. Sci. U. S. A.* **98,** 10566–10571 (2001).

62. Müller, K. *et al.* Synthesis of phycocyanobilin in mammalian cells. *Chem. Commun.* **49,** 8970–8972 (2013).

63. Toettcher, J. E., Gong, D., Lim, W. A. & Weiner, O. D. Light control of plasma membrane recruitment using the Phy–PIF system. *Methods Enzym.* **497,** 409–423 (2011).

64. Christie, J. M. *et al.* Plant UVR8 Photoreceptor Senses UV-B by Tryptophan-Mediated Disruption of Cross-Dimer Salt Bridges. *Science* **335,** 1492–1496 (2012).

65. Wu, D. *et al.* Structural basis of ultraviolet-B perception by UVR8. *Nature* **484,** 214–129 (2012).

66. Muller, K. *et al.* Multi-chromatic control of mammalian gene expression and signaling. *Nucleic Acids Res.* **41,** e124 (2013).

67. Schwerdtfeger, C. & Linden, H. VIVID is a flavoprotein and serves as a fungal blue light photoreceptor for photoadaptation. *EMBO J.* **22,** 4846–4855 (2003).

68. Elvin, M., Loros, J. J., Dunlap, J. C. & Heintzen, C. The PAS / LOV protein

VIVID supports a rapidly dampened daytime oscillator that facilitates entrainment of the Neurospora circadian clock. *Genes Dev.* **19,** 2593–2605 (2005).

69. Zoltowski, B. D. & Crane, B. R. Light Activation of the LOV Protein Vivid Generates a Rapidly Exchanging Dimer. *Biochemistry* **47,** 7012–7019 (2008).

70. Vaidya, A. T. *et al.* Structure of a Light-Activated LOV Protein Dimer That Regulates Transcription. *Sci. Signal.* **4,** ra50 (2012).

71. Lamb, J. S., Zoltowski, B. D., Pabit, S. A., Crane, B. R. & Pollack, L. Time-Resolved Dimerization of a PAS-LOV Protein Measured with Photocoupled Small Angle X-ray Scattering. *J. Am. Chem. Soc.* **130,** 12226–12227 (2008).

72. Lamb, J. S. *et al.* Illuminating Solution Responses of a LOV Domain Protein with Photocoupled Small-Angle X-Ray Scattering. *J. Mol. Biol.* **393,** 909–919 (2009).

73. Lokhandwala, J. *et al.* Structural Biochemistry of a Fungal LOV Domain Photoreceptor Reveals an Evolutionarily Conserved Pathway Integrating Light and Oxidative Stress. *Structure* **23,** 116–125 (2015).

74. Chen, X., Wang, X., Du, Z., Ma, Z. & Yang, Y. Spatiotemoral Control of Gene Expression in Mammalian cells and in Mice Using the lightOn System. *Curr. Protoc. Chem. Biol.* **5,** 111–129 (2013).

75. Ma, Z., Du, Z., Chen, X., Wang, X. & Yang, Y. Fine tuning the LightOn light-switchable transgene expression system. *Biochem. Biophys. Res. Commun.* **440,** 419–423 (2013).

76. Kawano, F., Suzuki, H., Furuya, A. & Sato, M. Engineered pairs of distinct photoswitches for optogenetic control of cellular proteins. *Nat. Commun.* **6,** 6256 (2015).

77. Nihongaki, Y., Kawano, F., Nakajima, T. & Sato, M. Photoactivatable CRISPR-Cas9 for optogenetic genome editing. *Nat. Biotechnol.* **33,** 755–760 (2015).

78. Lee, S. *et al.* Reversible protein inactivation by optogenetic trapping in cells. *Nat. Methods* **11,** 633–6 (2014).

Chapter II

Engineering Magnet system based on Assembly Domain

II-I Introduction

Our laboratory previously set out to improve VVD (Vivid), as this protein displays undesirable homodimerization[1]. Its homodimerization interface was engineered to develop two distinct Vivid variants, one positively and one negatively charged, named positive Magnet (pMag) and negative Magnet (nMag) respectively. When these two proteins bind to each other, electrostatic effect inside the interaction surface prevent unwanted homodimerization and providing selective light-induced heterodimerization. The Magnet system enabled manipulating cellular functions such as protein-protein interactions[2] and genome editing[3]. Nevertheless, there is still potential for improvement. For example, to enhance the nMag binding ability of pMagFast2, a pMag variant with fast kinetics, we introduced several pMagFast2 modules in tandem into a single construct, such as in pMagFast2(3×). However, we found that the expression level of our construct drastically decreased with increasing number of pMagFast2 integrated into a single construct.

In order to overcome this trade-off between binding ability and expression levels, here I used different assembly domains (ADs) to tag pMags in order to form an oligomeric complex. Out of the several domains tested, Ca^{2+}/calmodulin-dependent protein kinase IIα (CaMKIIα) association domain (CAD)-tagged pMag photoswitches exhibited strong nMag binding without a decrease in their expression levels. When I fused CAD to pMagFast2, the resulting CAD-pMagFast2 still retrained its fast switching kinetics, indicating that CAD did not interfere with the property of pMagFast2 by steric hindrance. Therefore, this assembly-domain based Magnet system is suited for photo-regulation of cellular signaling efficiently.

II-II Materials and methods

II-II-(i) Plasmid construction.

cDNAs encoding mouse CaMKIIα association domain (315−478), and human H ferritin full length (1−183) were synthesized by GenScript (Piscataway, NJ, USA). Both cDNA sequences were humanized. mCherry, DsRed-Express, and DsRed-Express2 were purchased from Clontech (Mountain View, CA, USA). All constructs were cloned into pcDNA3.1 (Invitrogen; Carlsbad, CA, USA).

II-II-(ii) Cell culture.

COS-7 and HEK293T cells (American Type Culture Collection (ATCC)) were cultured at 37°C under 5% CO_2 in Dulbecco's Modified Eagle Medium (DMEM; Invitrogen) supplemented with 10% fetal bovine serum (GIBCO, Carlsbad, CA, USA), 100 unit/ml penicillin and 100mg/ml of streptomycin (GIBCO). All cell culture was performed in this way, unless otherwise indicated.

II-II-(iii) Dish coating.

Glass-bottomed dishes (Matsunami Glass; Osaka, Japan) were coated with 25 μg/ml of human fibronectin (BD Biosciences; Franklin Lakes, NJ, USA) at room temperature for 1 h, and then washed twice with 2 ml of Milli-Q water.

II-II-(iv) TIRF translocation assay.

To conduct the plasma membrane translocation assay of assembled pMag probes using TIRF imaging, 1.5×10^4 cells COS-7 cells were plated on the well of

35-mm glass-bottomed dishes, and cultured for 24 h at 37°C in 5% CO_2. The cells were transfected with cDNAs encoding each assembled pMag probe and nMagHigh1-EGFP-CAAX at 1:1 ratio using X-tremeGENE 9 reagent (Roche Diagnostics; Mannheim, Germany) at 37°C. The total amount of DNA was 0.15 μg per dish. One day after transfection, the medium was replaced by DMEM culture medium supplemented with 10% FBS. The cells were maintained for 24 h at 28°C. Before imaging, the culture medium was replaced with Hanks' Balanced Salt Solution (HBSS; Grand Island Biological; Grand Island, NY, USA). Imaging was performed at room temperature with the 100× oil objective on the stage of an ECLIPSE Ti TIRF microscope (Nikon; Tokyo, Japan). Fluorescence images of mCherry or DsRed were taken using an optically pumped semiconductor laser at 561 nm (Coherent; CA, USA). Blue light irradiation was conducted using an optically pumped semiconductor laser (488 nm) at 1.0 mW for 50 ms.

II-II-(v) Confocal laser scanning microscopy imaging.

To obtain the confocal images of the plasma membrane translocation of assembled pMag activators, HEK293T cells were plated at 3.0×10^4 cells per well (for COS-7 at 1.5×10^4 cells per well) in 35-mm glass-bottomed dishes coated with fibronectin and cultured for 24 h at 37°C in 5% CO_2. The cells were transfected with cDNAs encoding each assembled pMag activator and nMagHigh1-EGFP-CAAX at 1:1 ratio using X-tremeGENE 9 reagent at 37°C. The total amount of DNA was 0.15 μg per dish. One day after transfection, the medium was replaced by DMEM culture medium supplemented with 10% FBS. The cells were maintained for 24 h at 28°C.

Before imaging, the culture medium was replaced with HBSS. Imaging was performed at with the 60× oil objective under the confocal laser-scanning microscope (FV1200, Olympus, Tokyo, Japan). During the experiment, the temperature of the sample was maintained at 37°C by a stage top incubator (Tokai Hit; Fujinomiya, Japan). EGFP, mCherry and DsRed were excited using a laser diode at 473 nm (Olympus) and at 559 nm (NTT Electronics; Yokohama, Japan), and using a solid-state laser at 515 nm (Coherent). Blue light irradiation was performed with a laser diode at 473 nm at 78 mW/cm^2.

II-II-(vi) A half-life evaluation for on and off kinetics.

In Figure 3D, and F in order to evaluate a half-life value, the extent of pMagFast2-mCh-CAD recruitment to the plasma membrane upon blue light irradiation was quantified based on the intensity of pMagFast2-mCh-CAD at the plasma membrane. Each time course of the change in mCherry intensity was fitted to an exponential saturation curve ($y = 1 - \exp(-kt)$) for **Fig. 3-2-4** and an exponential decay curve ($y = A \exp(-kt) + B$) for **Fig. 3-2-6** with the non-linear least-squares method, where y represents fluorescence intensity at time t, A and B are parameter, and k indicates the rate constant. The half-life value, $t_{1/2}$, was determined using the following equation ($t_{1/2} = \ln 2/k$).

II-III Results

II-III-(i) Assembly method to enhance the performances of the Magnet system

In order to improve the binding affinity of the components of the Magnet system (**Fig. 2-1-1**), I developed constructs with tandem-repeated pMags to create mCherry-tagged version of pMag (pMag-mCh), pMag (2×) (pMag(2×)-mCh), and pMag(3×) (pMag(3×)-mCh, **Fig. 2-1-2**), and expressed them in COS-7 cells. The expression levels of these constructs were inversely correlated to the number of pMag repetitions (**Fig. 2-1-3**). In order to overcome the trade-off between the expression level and nMag binding affinity, I assessed the possibility of incorporating several pMag repeats into a single oligomer through assembly domains (ADs; **Fig. 2-1-4**). This method would increase the binding affinity of pMag for its partner nMag, while at the same time keeping the molecular weight of the pMag probe low.

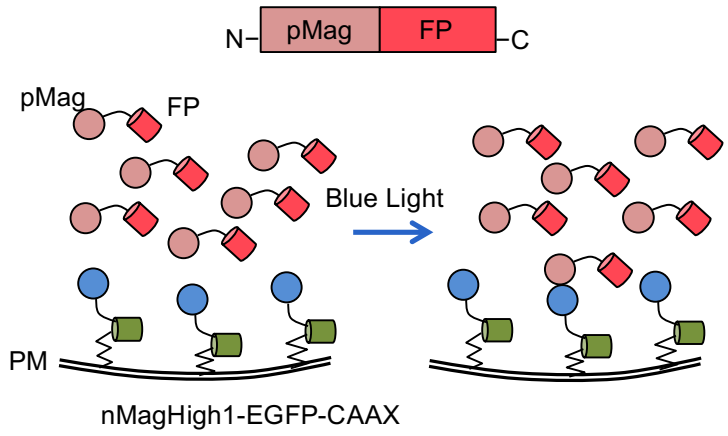

Figure 2-1-1. Fluorescent protein (FP)-tagged positive Magnet (pMag) binds with negative Magnet (nMag) tethered to the plasma membrane (PM) with a CAAX motif from K-ras in response to blue light.

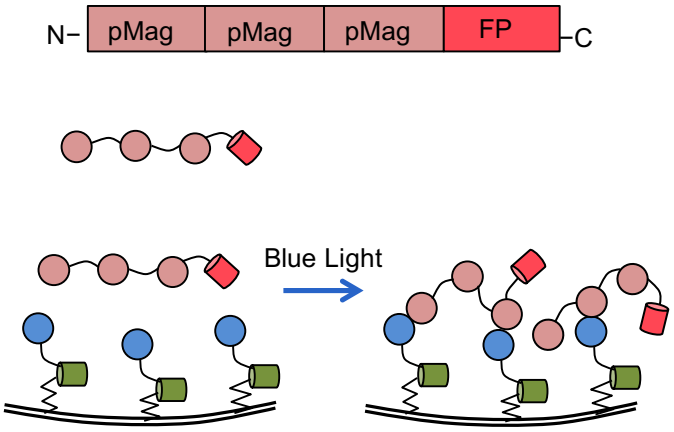

Figure 2-1-2. To gain the binding ability, some pMag molecules were tandemly repeated. Apparent binding ability (avidity) with nMag is increased.

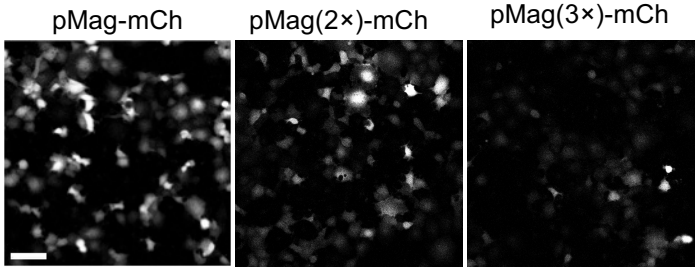

Figure 2-1-3. Tandem-repeated pMag were expressed in COS-7 cells. The expression level of pMag was decreased in a pMag number-dependent manner. This means the reduction in translocation efficiency. White bar indicates 100 μm.

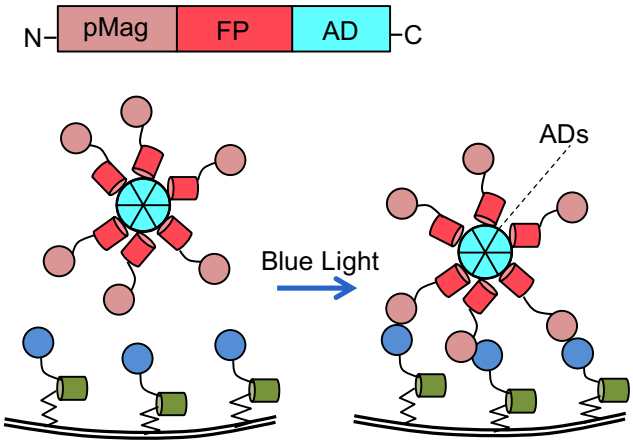

Figure 2-1-4. The strategy used in the present study. Assembly domains (ADs) gather and form oligomers including multiple pMags. pMag oligomerization through ADs is an alternative way to improve the avidity. (top) The primary structure of the pMag probe with AD.

Currently, several ADs are available (**Fig. 2-1-5**), such as the ones from the red fluorescent proteins DsRed-Express (DsRedEx) and DsRed-Express2 (DsRedEx2) (**Fig. 2-1-5 B**), which form homotetramers[4], the CaMKIIα association domain (CAD) (**Fig. 2-1-5A**), which forms a donut-like dodecamer[5], and ferritin (FTN) (**Fig. 2-1-5C**), which forms a spherical 24-mer[6]. I fused these ADs to pMag, creating the constructs named pMag-DsRed-Ex, pMag-DsRed-Ex2, pMag-CAD, and pMag-FTN.

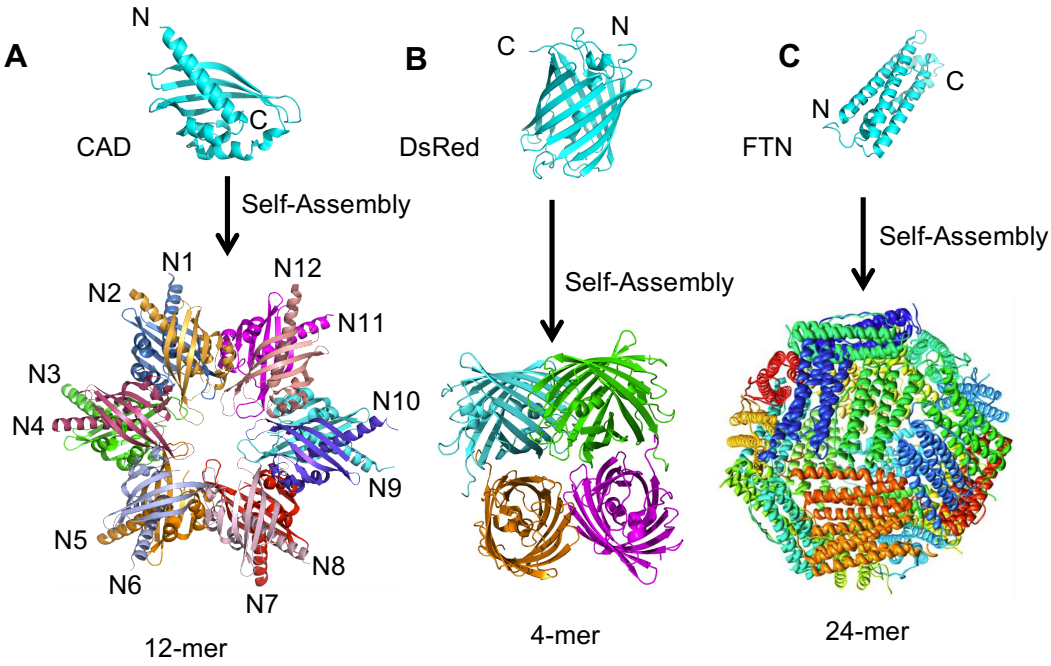

Figure 2-1-5 Three different Assembly domains (ADs) were separately tethered to pMag and examined in the present study. **(A)** CaMKIIα association domain (CAD) forms a donut-like 12-mer. **(B)** DsRed form a single tetramer, **(C)** ferritin induces a spherical 24-mer.

First, I checked the expression of pMag-CAD by transfecting COS-7 cells with an mCherry-tagged version of this construct (pMag-mCh-CAD). The expression level of pMag-mCh-CAD was comparable to that of pMag-mCh, pMag-DsRedEx2, and pMag-mCh-FTN (**Fig. 2-1-6**), indicating that my CAD approach solved the low protein expression problem seen with conventional tandem fusions.

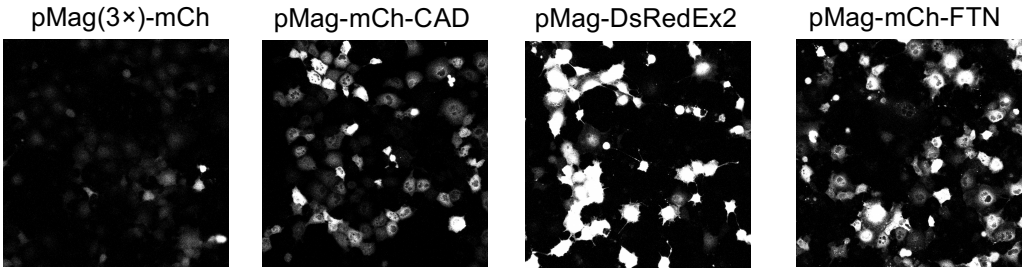

Figure 2-1-6. Low expression of tandem Magnet system and recovered high expression of AD-assembled pMag oligomer.

Next, I compared the association of different pMag variants to nMag using fluorescence confocal microscope imaging. I transfected pMag-mCh into HEK293T cells together with nMagHigh1-EGFP-CAAX, a high- affinity variant of nMag anchored to the plasma membrane via its CAAX motif[7–9]. Two days after transfection, the mCherry signal from pMag-mCherry exhibited an even cytosolic distribution, while I observed nMagHigh1-EGFP-CAAX at the plasma membrane (**Fig. 2-1-7**, upper panels). After irradiation of the whole cell with blue light for 5 sec, there was no significant translocation of pMag-mCh at the plasma membrane (**Fig. 2-1-7**, upper panels). Next, I examined the plasma membrane translocation of pMag(3×)-mCh and pMag-DsRedEx2. Both systems accumulated pMag at the plasma membrane after blue light irradiation. However, some cytosolic fluorescence was still present (**Fig. 2-1-7**,

middle panels). In contrast, the mCherry signal of pMag-mCherry-CAD clearly translocated to the plasma membrane after blue light irradiation (**Fig. 2-1-7**, lower panels). These results indicate that pMag-mCh-CAD has a far superior nMag binding ability compared to other pMags. Additionally, judging from the data showing that pMag did not translocate in the dark state, the Magnet system was not activated by the light used for cell observation (543 nm).

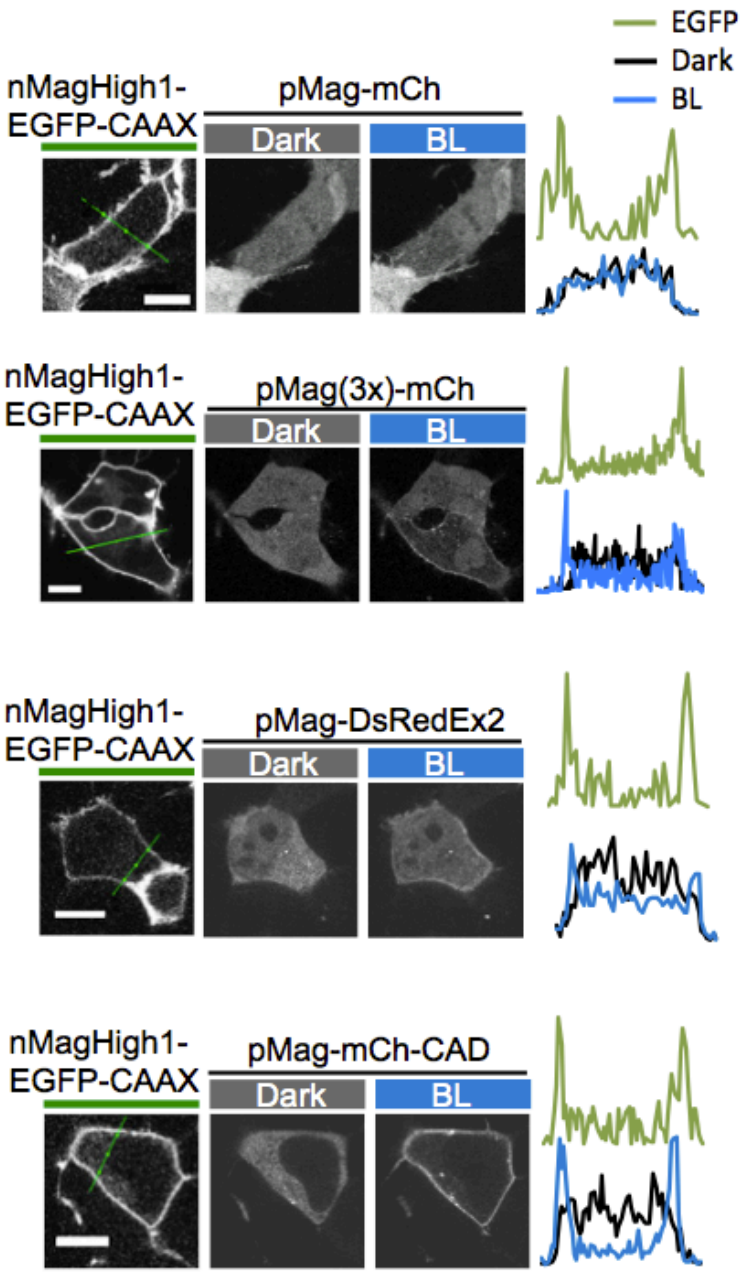

Figure 2-1-7. The observation of pMag translocation to the plasma membrane in HEK293T cells using confocal scanning microscopy (LSM710, Carl Zeiss). White bar indicates 10 μm. Left panels show the localization of nMagHigh1-EGFP-CAAX. Middle two panels show pMag translocation before and after blue light irradiation. Line profiles of right panels represent fluorescence intensities of EGFP (green) and mCherry (black and blue) measured along the green lines of the nMagHigh1-EGFP-CAAX images. pMag-mCh-CAD showed sharp translocation, which indicates its high binding ability between pMag and nMag.

To confirm the results, I used total internal reflection fluorescence (TIRF) microscopy to investigate the translocation of pMag to the plasma membrane, imaging MagHigh1-EGFP-CAAX and pMag-mCh-CAD expressed in COS-7 cells. Upon blue light irradiation, mCherry fluorescence increased, indicating that pMag-mCherry-CAD accumulated to the basal cell membrane (**Fig. 2-1-8**). Similarly, I examined other AD-fused pMags and pMags in tandem repeats. In order to evaluate the effect of assembly of each domain, the expression level fluorescence intensity was adjusted to that of pMagFast2(3×)-mCherry. I quantified the extent of pMag translocation to the plasma membrane as the ratio of mCherry or DsRedEx signal intensity before and after blue light irradiation (**Fig. 2-1-9**). The value of pMag-mCh-CAD (4.1 fold) was significantly higher than that of pMag-mCh (1.2 fold), pMag(3×)-mCh (3.0 fold), and pMag-mCh-FTN (2.8 fold). The position of the mCherry tag in the construct in relation to pMag did not significantly affect these values. For example, pMag-mCh-CAD had a value of 4.1 ± 0.3 fold, and mCh-pMag-CAD of 3.8 ± 0.3 fold. Taken together, these data demonstrated that CAD was superior to other ADs to control the Magnet system. I named then this as the CAD-Magnet system.

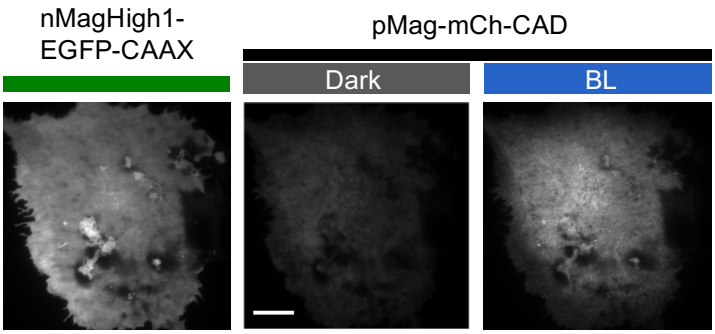

Figure 2-1-8. Typical TIRF translocation assay image. The binding abilities of pMag probes are evaluated by the fold increase of fluorescence intensity of TIRF image after/before irradiation with blue light. Anchor expression is confirmed by the image at the instant of irradiation with the blue light. Scale bar, 10 μm.

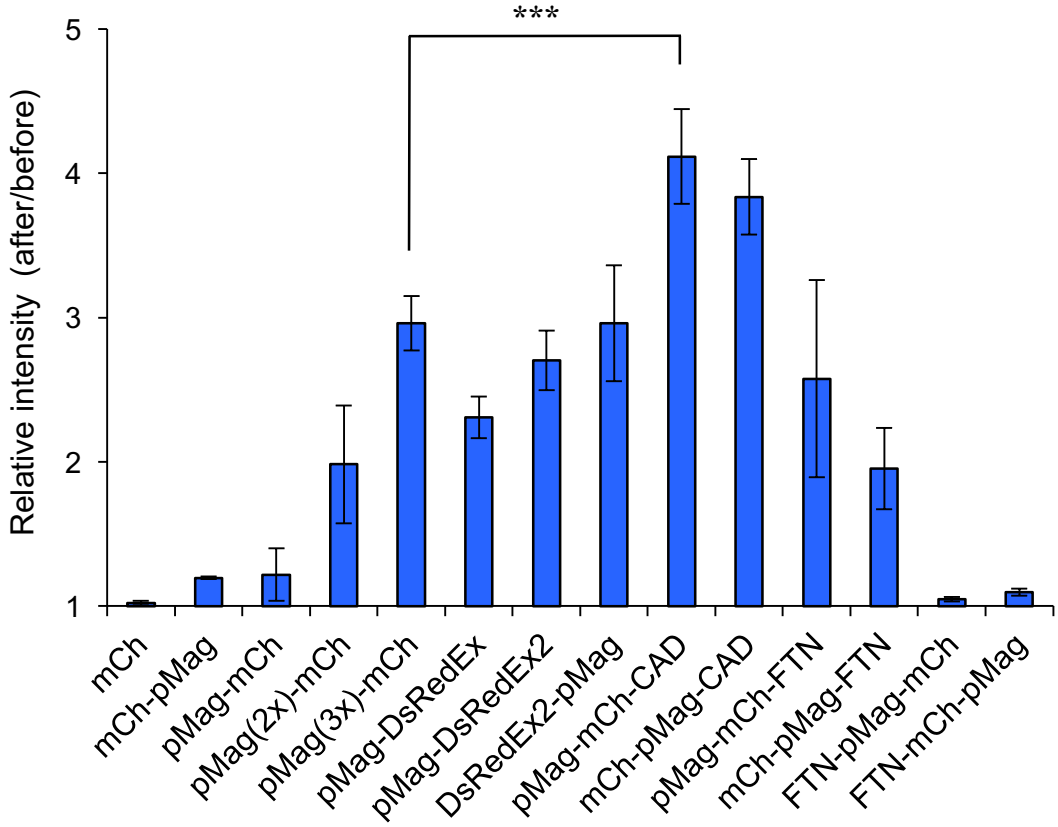

Figure 2-1-9. Comparison of the blue light-induced translocation to the plasma membrane among various Magnet systems, including the CAD-Magnet system. The results were shown as the mean ± standard error of the mean (s. e. m.). pMag-mCh-CAD showed the best fold increase of fluorescent intensity after/before blue-light irradiation, thereby, the highest binding ability. It showed superior affinity to pMag(3×)-mCh significantly. Asterisk indicates significant difference by unpaired two-tailed Student's t test, ***P < 0.001.

II-III-(ii) Kinetic study of the CAD-Magnet system

Next, in order to achieve quick photo-switching, I used the CAD-Magnet system with pMagFast2, a pMag variant with fast switch-off kinetics[2]. I expressed pMagFast2-mCh-CAD (F2C) and nMagHigh1-EGFP-CAAX together in HEK293T cells (**Fig. 2-2-1**). F2C exhibited even cytosolic distribution without blue light stimulation. After blue light irradiation, F2C was promptly translocated to the plasma membrane. After turning off the blue light, F2C returned to the cytosol. F2C was repeatedly recruited to the plasma membrane by switching on and off the blue light irradiation (**Fig. 2-2-1, 2-2-2**).

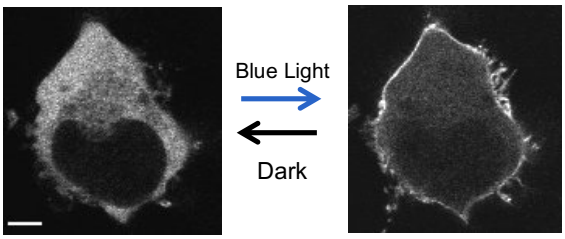

Figure 2-2-1. F2C translocates to plasma membrane (PM) upon blue-light exposure. In the dark, it dissociates from PM quickly. This process is repeatable.

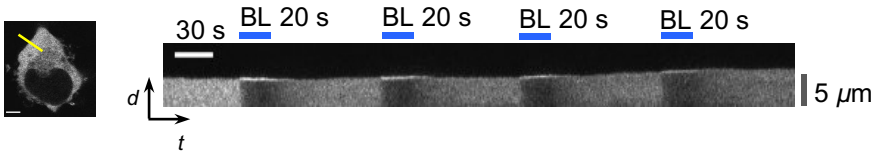

Figure 2-2-2. Kymograph at the yellow section of the left image. Upper blue lines indicate irradiation of blue light. White bar indicates 30 s. Irradiated with BL (blue light), F2C translocated instantly. When the light irradiation stopped, F2C dissociated into the cytosol rapidly.

Time-lapse imaging showed that the translocation of F2C to the plasma membrane was completed in a few seconds. Kymograph analysis showed that the half-life of the switch-on kinetics of F2C was 0.82 sec (**Fig. 2-2-3, 2-2-4**).

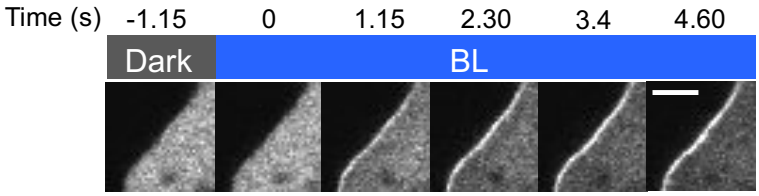

Figure 2-2-3. Magnified images of F2C translocation during the first irradiation with blue light all over the cell. In few seconds, F2C translocated completely to the plasma membrane. Scale bar, 5 μm.

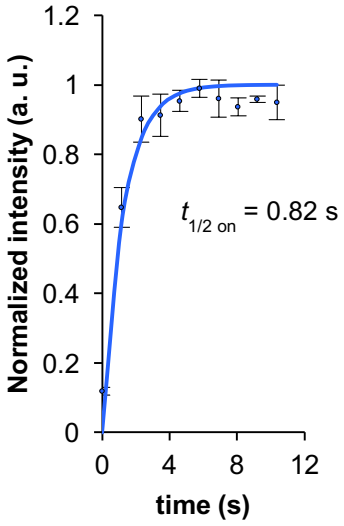

Figure 2-2-4. Analysis of the kinetics of F2C and nMagHigh1 binding. Normalized intensity was analyzed based on the F2C intensity at the plasma membrane. The $t_{1/2}$ was evaluated based on a curve fitted as a monoexponential function to the time course of the normalized intensity of F2C. The error bars indicate standard s.e.m. from three independent measurements.

Additionally, the half-life of the switch-off kinetics was 8.6 sec, comparable to that of pMagFast2(3x)-iRFP (6.8 sec) (**Fig. 2-2-5, 2-2-6**), indicating that CAD did not interfere with the fast switch-off kinetics of pMagFast2. This half-life of dissociation is superior to CRY2 (E349R) (2.5 min)[10], AsLOV2 (81 sec)[11], and iLID (< 30 sec)[12].

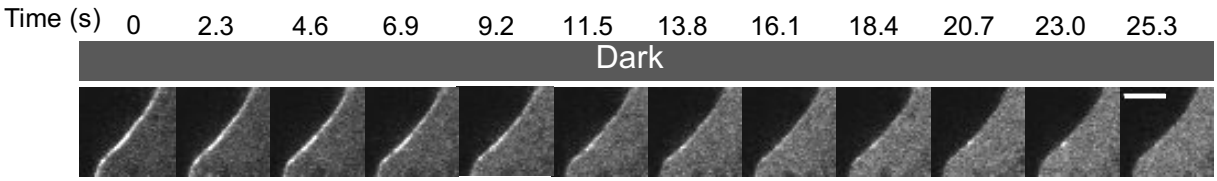

Figure 2-2-5. Magnified images of the recovery of F2C to the cytosol after the blue light was turned off. After around 10 seconds, F2C disappeared on the edge, which showed gradual dissociation of F2C from the PM. Scale bar, 5 μm.

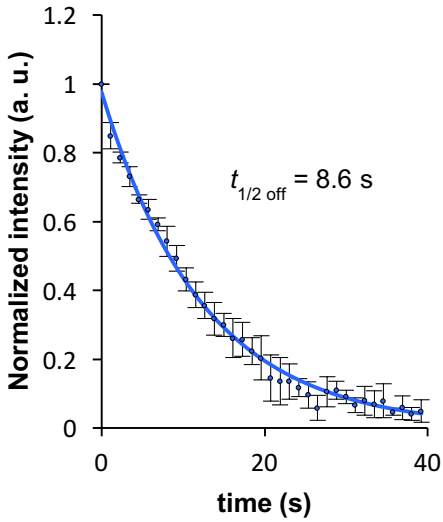

Figure 2-2-6. Analysis of the kinetics of F2C dissociation from nMagHigh1. Normalized intensity was analyzed based on the F2C intensity at the plasma membrane. The $t_{1/2}$ was evaluated based on a curve fitted as a monoexponential function to the time course of normalized intensity of F2C. The error bars indicate s.e.m. from three independent measurements.

I also performed experiments with subcellular blue light irradiation (**Fig. 2-2-7, 2-2-8**). I expressed F2C and nMagHigh1-EGFP-CAAX in HEK293T cells (**Fig. 2-2-7**). Upon blue light irradiation at the edge of the plasma membrane, I observed local translocation of F2C (**Fig. 2-2-7**). After I switched off the blue light irradiation, F2C quickly disappeared from the plasma membrane (**Fig. 2-2-7**).

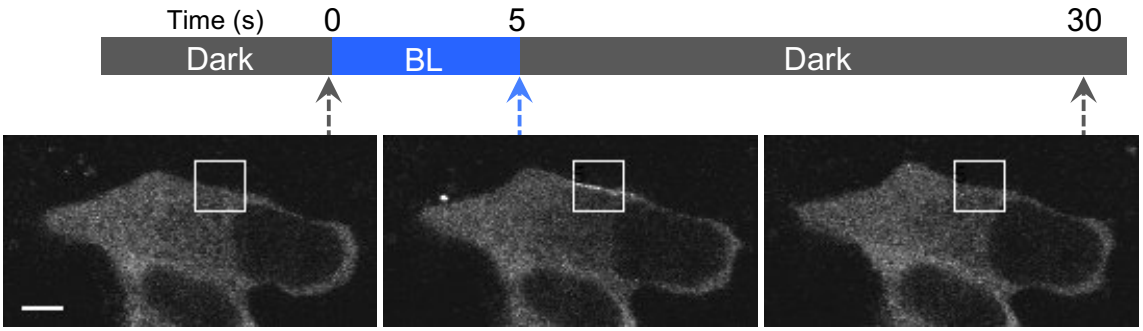

Figure 2-2-7. F2C translocation to the local region of the plasma membrane in HEK293T cells expressing nMagHigh1-EGFP-CAAX. The region surrounded by the white square was irradiated with blue light. At 5 s the local accumulation of F2C was observed there (middle panel). The white bar indicates 5 μm.

Next, localized blue light irradiation (**Fig. 2-2-8** bottom panel) resulted in the accumulation of F2C at the corresponding cell region (**Fig. 2-2-8** upper panel). Sequential subcellular blue light irradiation induced accumulation of F2C in those regions (**Fig. 2-2-8**). Taken together, these data indicated that F2C and nMagHigh1-EGFP-CAAX allowed for spatial and temporal control of protein subcellular localization in living cells.

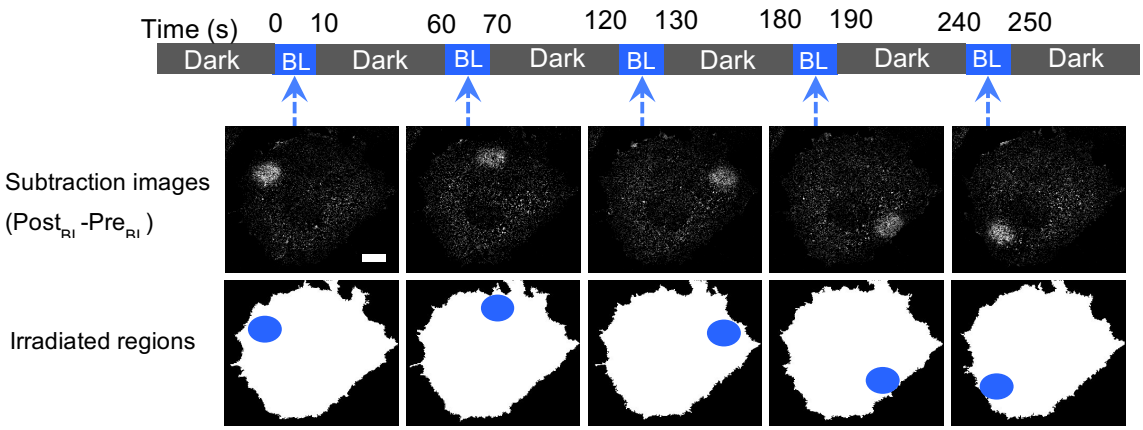

Figure 2-2-8. Local accumulation of F2C upon consecutive blue light irradiation at the different local regions of the plasma membrane in HEK293T cells expressing nMagHigh1-EGFP-CAAX. In the upper panel, increased F2C fluorescence was shown with the subtraction way, in which F2C fluorescence intensity before blue light irradiation was subtracted from the intensity after blue light irradiation. Blue ellipses at bottom panels indicate the irradiated regions. White bar indicates 10 *μ*m.

II-IV Discussion

By fusing the assembly domain to Magnet, I succeeded in creating the new optogenetic system, which shows high expression, high avidity, and fast kinetics. These advantages are important to make a superior optogenetic system, with efficient functional induction power and high spatiotemporal fidelity. High expression and high avidity are necessary for powerful translocation, and fast kinetics leads to the precise spatiotemporal control. For the assembly domain, I selected CaMKIIα association domain (CAD) over DsRed and ferritin, based upon the results of translocation assay. This success could be attributed to the conformation of the domain. DsRed and ferritin are full-length protein; on the other hand, CAD is truncated off the kinase domain. I replaced the kinase domain with the interaction domain (Magnet). The resulting new self-assembly type of optogenetic system showed sharp translocation to the plasma membrane and quick dissociation ($t_{1/2}$ = 8.6 s) from the membrane. This time constant is comparable to that of 6.8 s, as obtained in the previous study of Magnet (pMagFast2(3×)-iRFP), and the speed of dissociation was superior to that of CRY2 (E349R) (2.5 min)[10], AsLOV2 (81 s)[11], and iLID (< 30 s)[12]. Therefore, the new system is the fastest of all the other technologies. In addition, the photo-manipulation of the system was accurate about the subcellular translocation point and time of irradiation with light. The system also corresponded to the moving irradiated region and chased the spot.

In the following chapter, I discuss the application of the new system to inducible membrane recruitment of the representative GEF (guanine nucleotide exchange factor), Tiam1. The new system showed efficient and spatiotemporal induction of membrane morphology change.

II-V References

1. Zoltowski, B. D. *et al.* Conformational Switching in the Fungal Light Sensor Vivid. *Science* **316,** 1054–1057 (2007).

2. Kawano, F., Suzuki, H., Furuya, A. & Sato, M. Engineered pairs of distinct photoswitches for optogenetic control of cellular proteins. *Nat. Commun.* **6,** 6256 (2015).

3. Nihongaki, Y., Kawano, F., Nakajima, T. & Sato, M. Photoactivatable CRISPR-Cas9 for optogenetic genome editing. *Nat. Biotechnol.* **33,** 755–760 (2015).

4. Strack, R. L. *et al.* A noncytotoxic DsRed variant for whole-cell labeling. *Nat. Methods* **5,** 955–7 (2008).

5. Rosenberg, O. S., Deindl, S., Sung, R. J., Nairn, A. C. & Kuriyan, J. Structure of the autoinhibited kinase domain of CaMKII and SAXS analysis of the holoenzyme. *Cell* **123,** 849–860 (2005).

6. David M. Lawson & Harrison, P. M. Solving the structure of human H ferritin by genetically engineering intermolecular crystal contacts. *Nature* **349,** 541–544 (1991).

7. Sato, M., Ueda, Y., Takagi, T. & Umezawa, Y. Production of PtdInsP3 at endomembranes is triggered by receptor endocytosis. *Nat. Cell Biol.* **5,** 1016–1022 (2003).

8. Sato, M., Ueda, Y. & Umezawa, Y. Imaging diacylglycerol dynamics at organelle membranes. *Nat. Methods* **3,** 797–799 (2006).

9. Heo, W. Do *et al.* PI(3,4,5)P3 and PI(4,5)P2 lipids target proteins with polybasic clusters to the plasma membrane. *Science* **314,** 1458–61 (2006).

10. Taslimi, A. *et al.* Optimized second-generation CRY2–CIB dimerizers and photoactivatable Cre recombinase. *Nat. Chem. Biol.* 1–8 (2016). doi:10.1038/nchembio.2063

11. Zoltowski, B. D., Vaccaro, B. & Crane, B. R. Mechanism-based tuning of a LOV domain photoreceptor. *Nat. Chem. Biol.* **5,** 827–834 (2009).

12. Guntas, G. *et al.* Engineering an improved light-induced dimer (iLID) for controlling the localization and activity of signaling proteins. *Proc. Natl. Acad. Sci.* **112,** 112–117 (2015).

Chapter III

Optical control of membrane morphology

by the CAD-Magnet system

III-I Introduction

In this chapter, I applied the new Magnet system, engineered using the method explained in the previous chapter, to carry out effective induction of cellular signaling. To induce cellular signaling, I used the Dbl and pleckstrin homology (DH/PH) domain of the T-lymphoma invasion and metastasis 1 (Tiam1) protein, which enabled the regulation of spatiotemporal signaling of this GEF (guanine nucleotide exchange factor). This led to the formation of lamellipodia and cell ruffles as a result of actin reorganization induced by translocation of Tiam1 DH/PH domain driven by blue light irradiation. Thus, the local light exposure to CAD-Magnet system combined with 4D imaging allowed dissection of the ruffle dynamics on apical plasma membranes.

III-I-(i) Activation of Rac1 by Tiam1

In 1994, Tiam1 was identified as a GEF specific for Rac1 activation[1]. Tiam1 mainly acts upstream of Rac1 and regulates the Rac1-mediated signaling pathways, including cytoskeletal activities, endocytosis and membrane trafficking, cell polarity, cell migration, cell growth and survival, adhesion and invasion, metastasis, and carcinogenesis[2]. As illustrated in **Fig. 3-1-1**, Tiam1 is a large, multi-domain protein characterized by the presence of DH/PH domains, and thus belongs to the Dbl-like family of guanine exchange factors that regulate small GTPases of the Rho family. DH/PH domain is at the carboxy-terminal region and the minimal unit required for nucleotide exchange.

During activation, the Tiam1 DH domain contacts the switch region of Rac1 (**Fig. 3-1-2**). The DH-associated PH domains have several functions, including localization of Dbl-family proteins to plasma membranes and intramolecular regulation of exchange activity through the binding of specific membrane components.

Rac1 is one of the Rho GTPases, and upon activation, it activates Arp2/3 complex, mDia2, and PAK[3]. These signaling proteins induce actin polymerization. In particular, Arp2/3 complex initiates branching in the actin filaments, thereby forming net-like actin filaments, which are observed as lamellipodia on the edge of the plasma membrane. Lamellipodia are easily detectable by confocal laser-scanning microscopy[4–7]. Additionally, in the preceding study (engineering the Magnet system), the response of membrane recruitment of Tiam1 DH/PH domain (the formation of lamellipodia) was clear[7]. Therefore, I selected the Tiam1 signaling pathway as the target of the improved Magnet system, of which the efficiency was tested in its application to induction of lamellipodia.

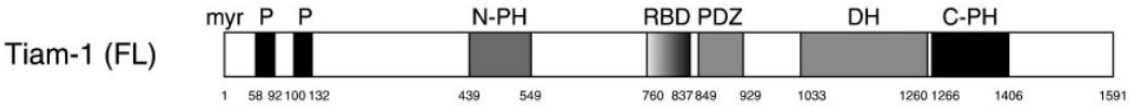

Figure 3-1-1. The primary structure of Tiam1 (full length). The DH and C-PH domain was employed for induction of cellular signaling in this study. DH domain grab the switch domain of Rac1 and activate Rac1.

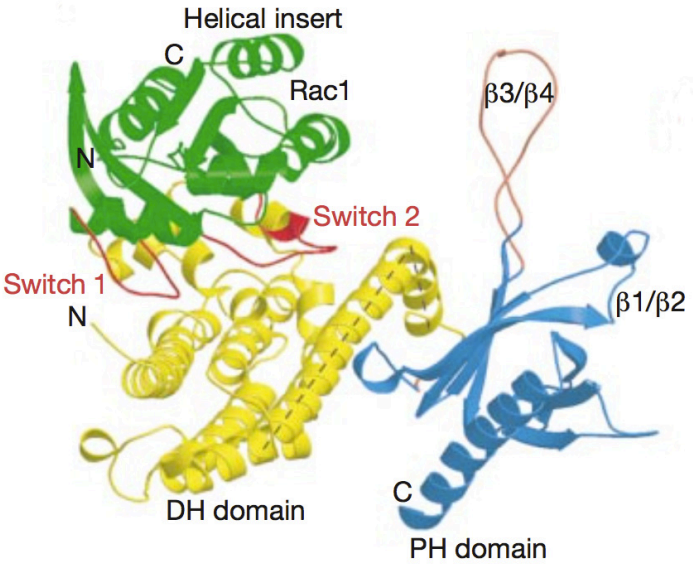

Figure 3-1-2. The structure of the Tiam1/Rac1 complex. Switch regions of Rac1 are red; the rest of the G protein is green. Tiam1 DH and PH domains are yellow and blue, respectively; disordered regions are orange.
DH domain grabs the switch regions of Rac1 and activate it.

III-II Materials and methods

III-II-(i) Plasmid construction.

Mouse Tiam1 cDNA was obtained from Addgene (22277) (Cambridge, MA, USA). A DH/PH domain (1033−1406) of Tiam1 was prepared by polymerase chain reaction (PCR). All constructs were cloned into pcDNA3.1 (Invitrogen; Carlsbad, CA, USA).

III-II-(ii) Cell culture and dish coating.

They were prepared as described above (in Chapter II-II, p.49).

III-II-(iii) Confocal laser scanning microscopy imaging.

To observe morphological changes in the plasma membrane using assembled pMag activators, COS-7 cells were plated at 0.3×10^4 cells per dish on glass-bottomed dishes coated with fibronectin. The cells were transfected with both Lifeact-mCherry-P2A-Tiam1-pMagFast2-CAD and nMagHigh1-EGFP-CAAX plasmids at 1:9 ratio using X-tremeGENE 9 reagent. The total amount of DNA was 0.15 μg per dish. 24 hours after transfection, the medium was replaced by DMEM culture medium supplemented with 10% FBS. The cells were maintained for 24 h at 28°C. Imaging was performed at 37°C with the 63× oil objective lens under the confocal laser-scanning microscope (LSM710 Carl Zeiss, Germany). During the experiment, the temperature of the sample was maintained at 37°C by a stage top incubator. EGFP, mCherry and DsRed-Express2 were excited using a multi-line Argon

laser (514 nm) and a HeNe laser (543 nm). Blue light irradiation was performed with a multi-line Argon laser (488 nm) at 0.25 mW.

4D image in **Fig. 3-3-7**, **3-3-12** was taken at 37°C with the 63× oil objective under the white light laser scanning confocal microscope (TCS SP8 X, Leica Microsystems, Germany). Each image was composed from stacking of 17 slices of *X*−*Y* images; 17 slices cover 12.8 μm.

III-III Results

III-III-(i) Optical control of membrane morphology by the CAD-Magnet system

Previous reports indicate that plasma membrane translocation of Tiam1[4,5], a GEF regulating Rac1 activation, through its DH/PH domain induces the development of membrane ruffles and lamellipodia[2,4,5,8]. In order to precisely control lamellipodia formation, I fused the Tiam1 DH/PH domain to pMagFast2(3×) (TiamF2(3×); **Fig. 3-3-1**). To visualize actin dynamics, I fused Lifeact, a 17 amino acid actin-binding peptide[9], to mCherry (LifemCh). Both constructs flanked a P2A peptide (LifemCh-P2A-TiamF2(3×)), enabling equal expression of both proteins[10]. I expressed LifemCh-P2A-TiamF2(3×) and nMagHigh1-EGFP-CAAX in COS-7 cells, and after whole-cell irradiation with blue light, LifemCh labeled the periphery of the cell, indicating lamellipodia generation at the plasma membrane (**Fig. 3-3-1**).

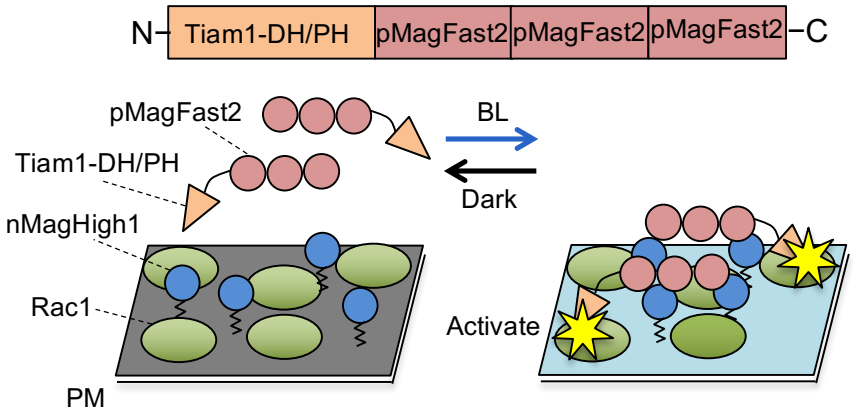

Figure 3-3-1. Schematic of Tiam1-pMagFast2(3×). A DH/PH domain of Tiam1 was fused with pMagFast2(3×). The activator can translocate to the plasma membrane where nMagHigh1-EGFP-CAAX was tethered in response to blue light, and induce ruffles and lamellipodia through Rac1 activation.

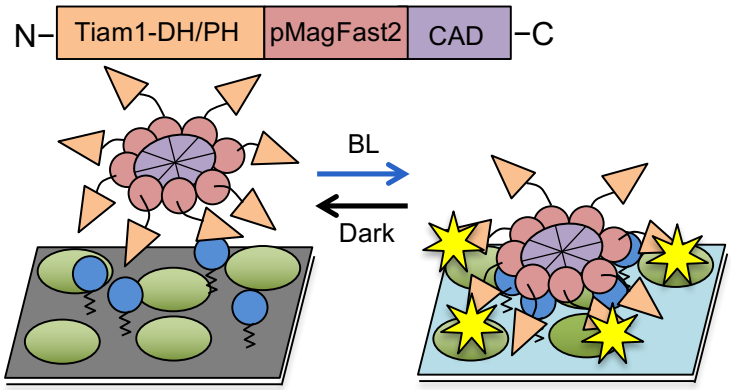

Figure 3-3-2. Schematic of Tiam1-pMagFast2-CAD (TiamF2C). Twelve Tiam1 molecules can be incorporated into a F2C complex. The TiamF2C is expected to efficiently lead to ruffles and lamellipodia through Rac1 activation on the plasma membrane in a blue light-dependent manner.

Next, I also examined pMagFast2-CAD. As in the case of TiamF2(3×), I fused the Tiam1 DH/PH domain to pMagFast2-CAD (TiamF2C) (**Fig. 3-3-2**), linked it to Lifeact-mCherry through P2A (LifemCh-P2A-TiamF2C) and expressed it together with nMagHigh1-EGFP-CAAX in COS-7 cells. After blue light irradiation, these cells exhibited stronger plasma membrane expansion and lamellipodia formation than those expressing LifemCh-P2A-TiamF2(3×) (**Fig. 3-3-3**).

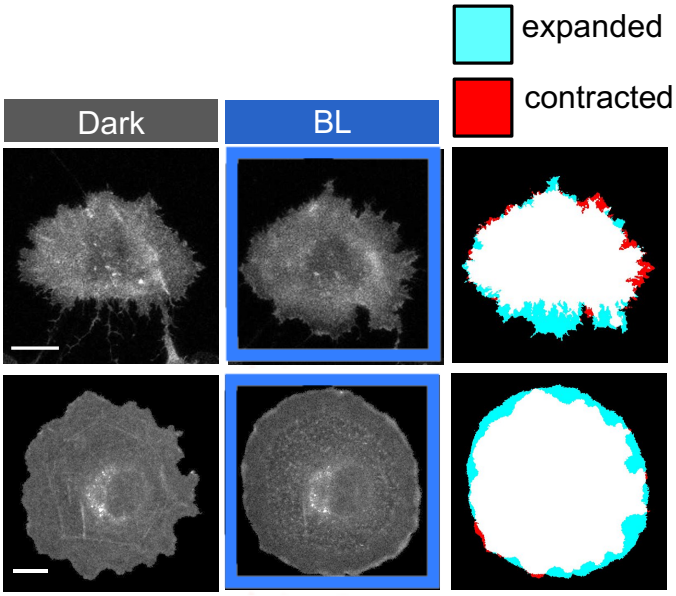

Figure 3-3-3. Effect of the Tiam1-Magnet system on actin regulation and cell membrane expansion in COS-7 cells upon irradiation of the whole cell with blue light for 10 min. Actin dynamics were observed with Lifeact-mCherry. Photo-induced lamellipodia by TiamF2(3×) (upper) and by TiamF2C (lower). Cyan area is expanded, and red area is contracted region. Scale bar, 20 *μ*m.

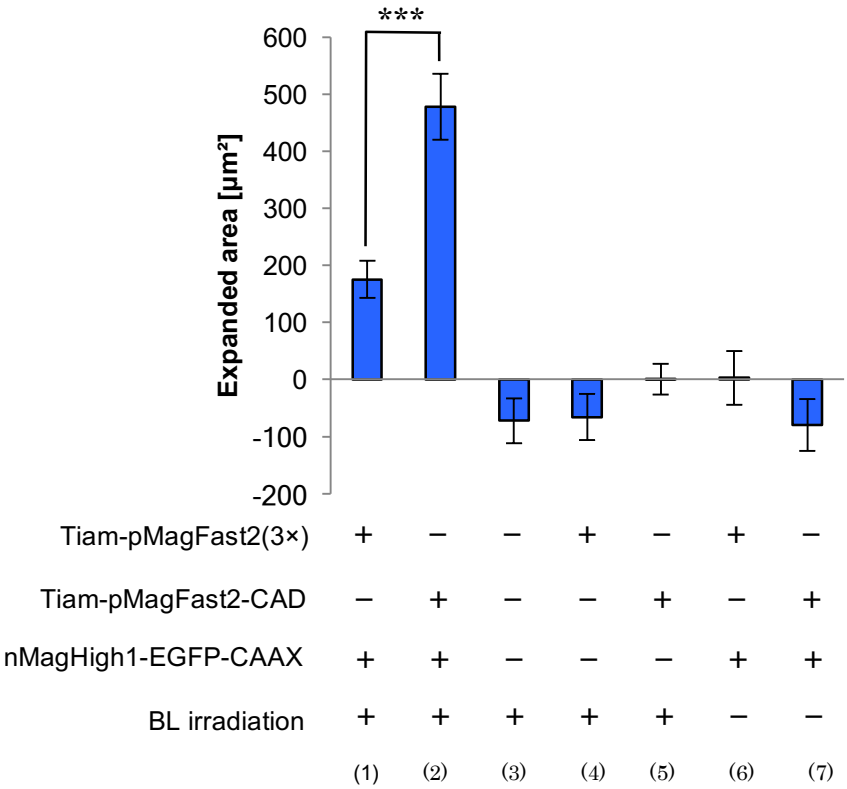

Figure 3-3-4. Cell area change was analyzed by the change of the cell shape. (1) and (2) are the data of TiamF2(3×) and TiamF2C respectively. TiamF2C showed 2.6-fold higher data than that of TiamF2(3×). Data represent average and s.e.m. Asterisk indicates significant differences by unpaired two-tailed Student's t-test, $^{***}P<0.001$.

To analyze the extent of cell expansion as a measure of lamellipodia formation, I measured the cell area before and after irradiation (**Fig. 3-3-4**). LifemCh-P2A-TiamF2C induced an expansion 2.6 times higher than that induced by LifemCh-P2A-TiamF2(3×) (**Fig. 3-3-4**). Thus, the synergistic effect resulting from improvement of the expression level of the Magnet system and converging the signaling molecules by CAD induced a more robust output. In contrast, I observed no significant cell area expansion without blue light irradiation (**Fig. 3-3-4** (6) and (7)). Expression of LifemCh-P2A- TiamF2C or LifemCh-P2A-TiamF2(3×) in the absence of nMagHigh1-EGFP- CAAX did not induce cell area expansion (**Fig. 3-3-4 (4)** and **(5)**). Similarly, blue light irradiation alone induced no cell area expansion (**Fig. 3-3-4 (3)**).

I have previously found that blue light irradiation on a portion of a cell expressing the Magnet system results in the plasma membrane expansion in the corresponding side and retraction on the other side[7]. This phenomenon is interpreted as a result that the light-irradiated expanding membrane pulled the other side of the cell via actin filaments. Therefore, here I irradiated the center of the cell with blue light. This focal irradiation resulted in the retraction of the peripheral plasma membrane as expected (**Fig. 3-3-5**). As for cell expansion, LifemCh-P2A-TiamF2C induced more membrane retraction than LifemCh-P2A-TiamF2(3×) (**Fig. 3-3-6 (1)**). Blue light irradiation alone did not lead to cell membrane retraction (**Fig. 3-3-6 (3)**).

LifemCh-P2A-TiamF2C and LifemCh-P2A-TiamF2(3×) did not induce cell membrane retraction without the expression of nMagHigh1-EGFP-CAAX (**Fig. 3-3-6 (4), (5)**). Collectively, these data indicate that LifemCh-P2A-TiamF2C is a robust optogenetic tool compared to LifemCh-P2A-TiamF2(3×) to induce Tiam1-mediated actin regulation. Additionally, a basal effect is not induced by overexpression of Tiam-pMagFast2-CAD, as shown in the dark-state images in **Fig. 3-3-3** lower and **Fig. 3-3-5**.

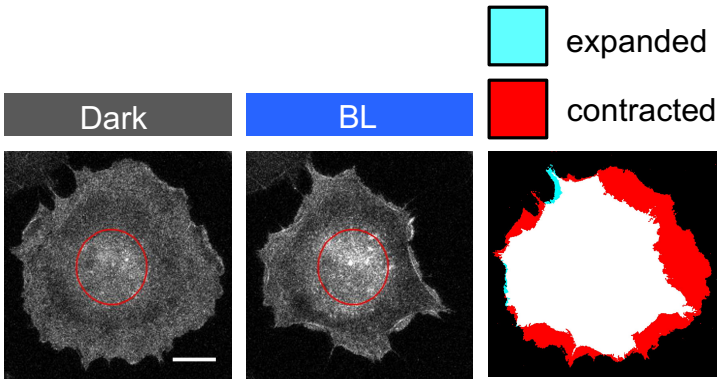

Figure 3-3-5. The effect of the TiamF2C on actin regulation and cell membrane retraction in COS-7 cells when the center region of the cell was irradiated with blue light for 10 min. Scale bar, 20 *μ*m.

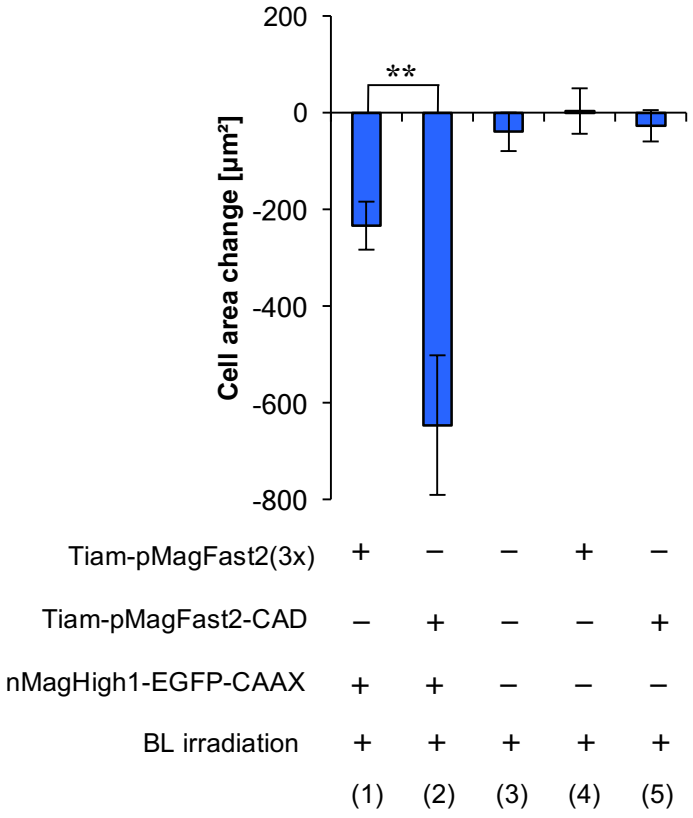

Figure 3-3-6. The extent of cell membrane retraction was analyzed by the change in kymograph of cell shape. TiamF2C showed 2.9-fold higher data than that of TiamF2(3×). Data represents average and s.e.m. Asterisk indicates significant differences by unpaired two-tailed Student's t-test, $^{**}P<0.015$.

III-III-(ii) 4D imaging of optically inducing apical ruffles

Finally, I used 4D imaging to observe the plasma membrane after optogenetic perturbation by LifemCh-P2A-TiamF2C. I expressed LifemCh-P2A-TiamF2C and nMagHigh1-EGFP-CAAX in COS-7 cells and irradiated a local region of the cell with blue light (**Fig. 3-3-7**). After irradiation, ruffles rose from the apical plasma membrane resulting in cell membrane expansion at the edge close to the irradiated region (**Fig. 3-3-7, 3-3-8**).

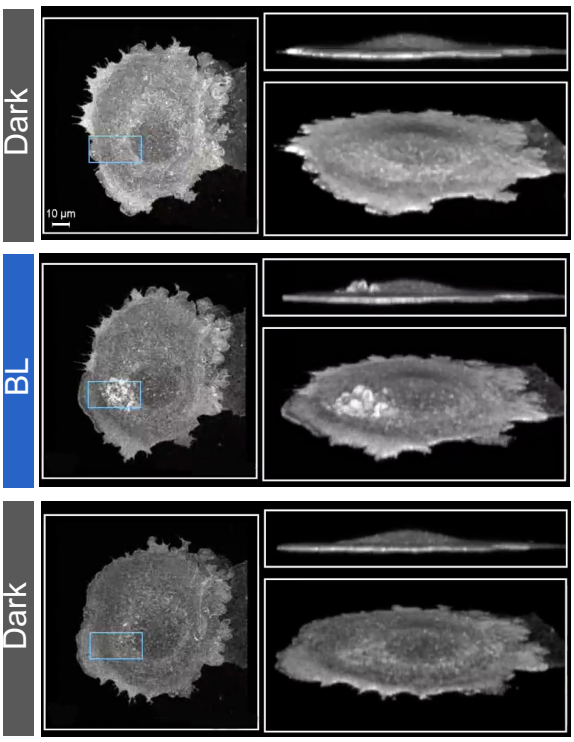

Figure 3-3-7. 4D image of local ruffles visualized by Lifeact-mCh in COS-7 cells expressing TiamF2C and nMagHigh1-EGFP-CAAX. The region surrounded by a blue square was irradiated with blue light for 20 min. Just after irradiation of blue light, apical ruffles were formed inside the exposure region. A few minutes after turning off the light, ruffles disappeared. White bar shows 10 μm. The major apical ruffles were observed in three out of six COS-7 cells expressing the TiamF2C Magnet version.

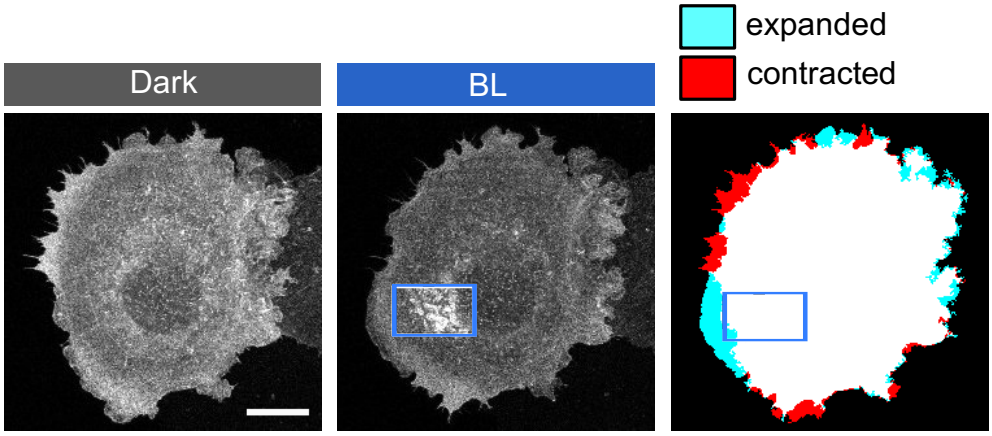

Figure 3-3-8. Cell membrane expansion following blue light irradiation at the blue square for 20 min. The cell is expressing TiamF2C. White bar shows 20 μm. At the same time, inside the blue square apical ruffles were observed.

The ruffles were spatially and temporally confined and did not spread to other regions. Magnification of the activated region by irradiated TiamF2C revealed that the vertical ruffle walls were 5 μm in height (**Fig. 3-3-9**) and that they formed actin rings (**Fig. 3-3-10**).

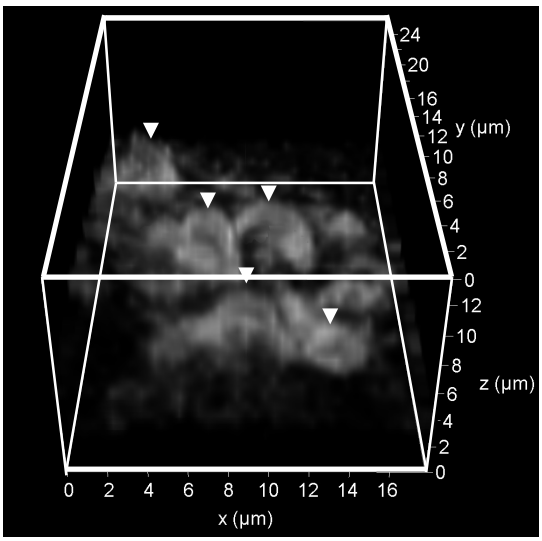

Figure 3-3-9. A snapshot of ruffle walls indicated by white arrowheads in the activated area of the cell expressing TiamF2C.

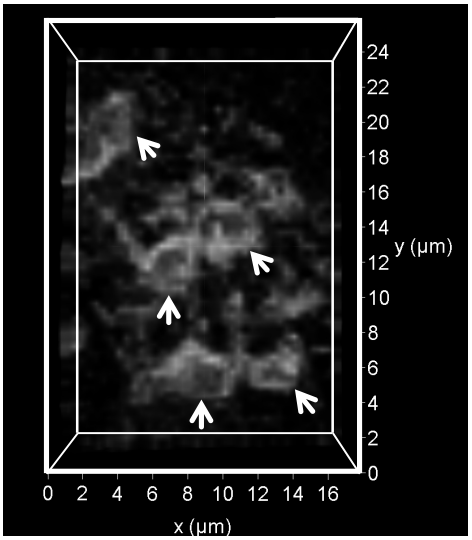

Figure 3-3-10. Actin ring formation at the apical plasma membrane as shown by white arrows after ruffle walls overhung on the apical plasma membrane in the activated area of the cell expressing TiamF2C.

LifemCh-P2A-TiamF2(3×) was also tested. The lamellipodia were observed as well as the case of LifemCh-P2A-TiamF2C (**Fig. 3-3-11**). However, I did not detect apical ruffles (**Fig. 3-3-12**). These data indicate that only the CAD Magnet system enables the induction of apical ruffles. Thus, 4D experiment is one of the specific applications of the novel pMag assembly system. The potential of the new Magnet system, TiamF2C, is that it would be useful to enhance the signal transduction by concentrating the effectors at the limited region on the plasma membrane. Since mtheCAD-Magnet system is constructed based on rational design, we can avoid the issues like the inactivation by CRY2 self-oligomerization[11] and, in an opposite way, the basal activation of signal transduction by CRY2 self-oligomerization.

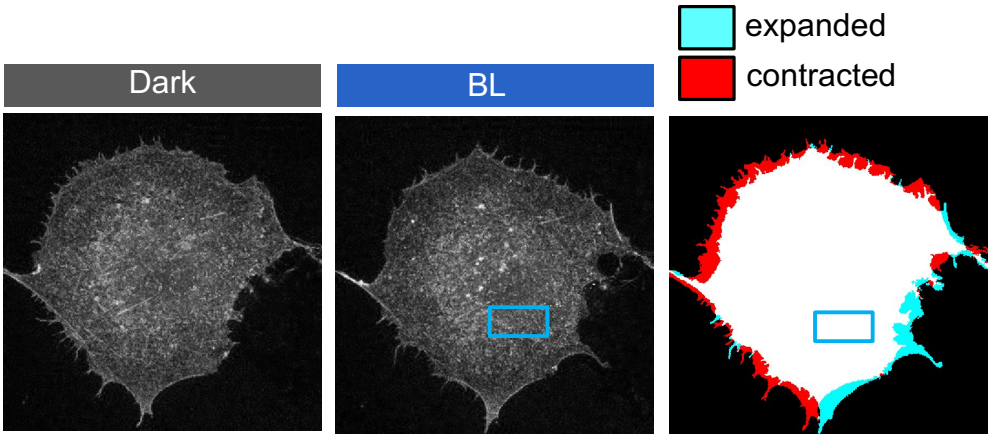

Figure 3-3-11. Cell membrane expansion following blue light irradiation at the blue square for 20 min. The cell is expressing TiamF2(3×). Expansion was also induced by TiamF2(3×), but apical ruffles were not observed.

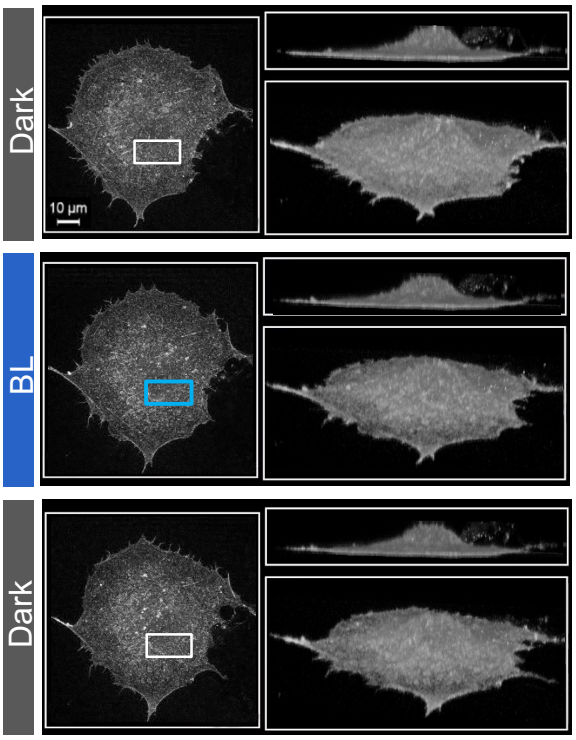

Figure 3-3-12. 4D image of local ruffles visualized by Lifeact-mCh in COS-7 cells expressing TiamF2(3×) and nMagHigh1-EGFP-CAAX. The region surrounded by a blue square was irradiated with blue light for 20 min. White bar shows 10 *μ*m. The major apical ruffles were not observed in any cells expressing the TiamF2(3×) Magnet version (*n* = 6).

Time course analysis of the *z*-cross section (shown with a blue rectangle in **Fig. 3-3-13A**) showed that actin ring formation at the apical membrane completed within 2 min (**Fig. 3-3-13B**, top panels). The *x*-cross section (shown with a green rectangle in **Fig. 3-3-13A**) showed that the ruffles grew vertically (**Fig. 3-3-13B**, middle panels). Then, the ruffle overhung on the apical plasma membrane within 2 min, and finally formed a dome structure. The *y*-cross section (shown with a red rectangle in **Fig. 3-3-13A**) indicated that the bottom and rim part of the ruffle, which was indicated as white arrowheads on the time of 65.3 sec, appeared earlier than top part (**Fig. 3-3-13B** lower panels). The 4D imaging analysis allowed me to detail the whole apical ruffle formation process (**Fig. 3-3-13C**). In summary, these results demonstrated that the CAD-Magnet system displayed strong dimer binding, fast photoswitching kinetics, and the ability to drive the localization of multiple effectors. The CAD-Magnet system in combination with 4D imaging enabled me to describe the process of ruffle formation in detail.

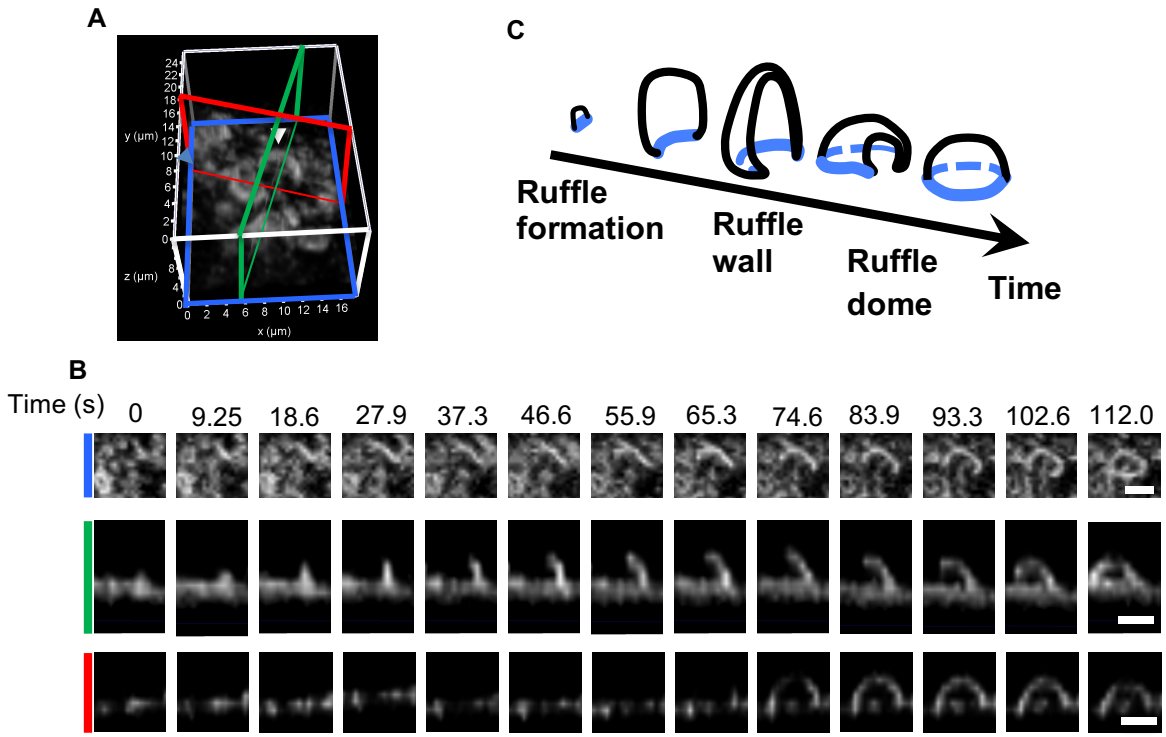

Figure 3-3-13. (A) Cross section analysis of a ruffle on the apical plasma membrane. (B) Time course of the cross sections of the ruffle specified with a white arrow head in Figure 7A. The upper, middle, and bottom cross sections were obtained as shown with blue, green, and red rectangles in Figure 7A, respectively. White bars indicate 2 μm. (C) Schematic representative from ruffle formation to ruffle dome. Blue lines indicate filamentous actin at the plasma membrane.

III-IV Discussion

In chapter 2, the creation of a new Magnet system (TiamF2C) with powerful (high avidity) and spatiotemporal (fast kinetics) advantages has been discussed. In this chapter, the application of this system to inducible translocation of Tiam1 that is the selective GDP/GTP exchange factor (GEF) for Rac1, representative Rho GTPase, has been mentioned. As compared to tandem type system (TiamF2(3×)), TiamF2C showed more powerful induction of lamellipodia and shrinking of the plasma membrane. These results indicate that the CAD-Magnet system is a highly efficient tool to regulate Rac1 at least. Similarly, the system could be applied to other GEFs, GTPase activating proteins (GAPs), or GDP dissociation inhibitors (GDIs) to regulate various small GTPases efficiently. The effect of introducing CAD derives from the high avidity from multivalency of pMag and the number of converged functional domains. TiamF2C also showed high spatiotemporal control, which derives from fast kinetics of pMagFast2. In other words, the self-assembly domain-based Magnet (photoswitch) system showed excellent efficacy and fidelity to light. Therefore, I demonstrated that the self-assembly method increased the avidity and multivalency of the photoswitch system to regulate cellular signaling efficiently. Fast kinetics is an inherent character of pMagFast2, and fusing of CAD to pMagFast2 does not cause steric hindrance of the interaction with nMagHigh1 on the plasma membrane.

As the next measurement, a 4D movie of apical ruffles, induced with light

exposure to the CAD-Magnet system, was recorded. It revealed the time-lapse dynamics, shape-change, and disappearance of apical ruffles creation. The ruffles appeared immediately after the irradiation of light, and disappeared within a couple of minutes after removal of light. This indicates the high-spatiotemporal resolution of the new system. With another photoswitch system, iLID, Rac1 was regulated and lamellipodia were induced efficiently[6]; however, apical ruffles were not reported in this[6] as well as in other studies (membrane recruitment of Tiam1 or Rac1)[5,7,12,13]. They pointed out only that their systems enabled to control the shape of the cell edge with light at will. Therefore, the apical ruffles produced by optical activation of Rac1 were newly measured by 3D live imaging and described in this study. The 3D dynamics of apical ruffles was firstly observed with my research using light. In addition, through this result, the CAD-Magnet system demonstrates its powerful and spatiotemporal manipulation of cellular signaling.

III-V References

1. Habets, G. G. M. *et al.* Identification of an invasion-inducing gene, Tiam-1, that encodes a protein with homology to GDP-GTP exchangers for Rho-like proteins. *Cell* **77,** 537–549 (1994).

2. Boissier, P. & Huynh-Do, U. The guanine nucleotide exchange factor Tiam1: A Janus-faced molecule in cellular signaling. *Cell. Signal.* **26,** 483–491 (2014).

3. Heasman, S. J. & Ridley, A. J. Mammalian Rho GTPases: new insights into their functions from in vivo studies. *Nat. Rev. Mol. cell Biol.* **9,** 690–701 (2008).

4. Inoue, T., Heo, W. Do, Grimley, J. S., Wandless, T. J. & Meyer, T. An inducible translocation strategy to rapidly activate and inhibit small GTPase signaling pathways. *Nat. Methods* **2,** 415–418 (2005).

5. Levskaya, A., Weiner, O. D., Lim, W. A. & Voigt, C. A. Spatiotemporal control of cell signalling using a light-switchable protein interaction. *Nature* **461,** 997–1001 (2009).

6. Guntas, G. *et al.* Engineering an improved light-induced dimer (iLID) for controlling the localization and activity of signaling proteins. *Proc. Natl. Acad. Sci.* **112,** 112–117 (2015).

7. Kawano, F., Suzuki, H., Furuya, A. & Sato, M. Engineered pairs of distinct photoswitches for optogenetic control of cellular proteins. *Nat. Commun.* **6,** 6256

(2015).

8. Michiels, F. *et al.* Regulated Membrane Localization of Tiam1, Mediated by the NH2-terminal Pleckstrin Homology Domain, Is Required for Rac-dependent Membrane Ruffling and C-Jun NH2-terminal Kinase Activation. *J. Cell Biol.* **137,** 387–398 (1997).

9. Riedl, J. *et al.* Lifeact: a versatile marker to visualize F-actin. *Nat. Methods* **5,** 605–607 (2008).

10. Kim, J. H. *et al.* High cleavage efficiency of a 2A peptide derived from porcine teschovirus-1 in human cell lines, zebrafish and mice. *PLoS One* **6,** e18556 (2011).

11. Taslimi, A. *et al.* An optimized optogenetic clustering tool for probing protein interaction and function. *Nat. Commun.* **5,** 4925 (2014).

12. Wu, Y. I. *et al.* A genetically encoded photoactivatable Rac controls the motility of living cells. *Nature* **461,** 104–108 (2009).

13. Yazawa, M., Sadaghiani, A. M., Hsueh, B. & Dolmetsch, R. E. Induction of protein-protein interactions in live cells using light. *Nat. Biotechnol.* **27,** 941–945 (2009).

Chapter IV

General Conclusion

My goal is to develop rational design-based photoswitches to reliably induce cellular signaling in living cells. For this purpose, the first version of the Magnet system was previously developed with 1:1 pMag/nMag heterodimer formation. Since the molecular size of each half was small, the Magnet system was suitable for use in applications such as protein complementation, including Photoactivatable CRISPR–Cas9,[1] and Photoactivatable Cre–loxP recombination system.[2] Additionally, the Magnet system possesses another advantage, such as fast pMag/nMag kinetics (for example, the pair of pMagFast2 and nMagHigh1), as described elsewhere,[3] which was ideal for applying the translocation technology to the activation of cellular signaling. However, instead of fast kinetics, the pMag/nMag binding ability was relatively low. Additionally, we found that the expression level of this construct decreased with increasing number of pMagFast2 molecules integrated into a single construct such as pMagFast2(3×). Therefore, further enhancement of the Magnet system was needed. I previously engineered the Magnet system from the fungal photoreceptor Vivid[4]. The combination of pMagFast2 and nMagHigh1 resulted in fast switch-on and off kinetics, but also in reducing their binding affinity. In order to solve this issue, I adopted ADs. CAD-fused pMag oligomerized after translation. This kept its molecular weight lower than constructs with tandem repeated pMags, leading to a great improvement in its expression. Additionally, the oligomerization of twelve pMags by CAD also enhanced their binding to nMag compared to existing pMag and pMag(3×). With these

modifications, the performance of the previous Magnet system is improved greatly. Furthermore, the CAD-Magnet system also makes it possible to localize effector proteins, such as Tiam1, in regions irradiated with blue light. Relocalization of the Tiam1 dodecamer could effectively create membrane ruffles and lamellipodia through Rac (**Fig. 3-3-2**). Therefore, the CAD-Magnet-Tiam1 system induced cell membrane expansion and retraction more robustly than tandem-repeated Magnet-Tiam1 (**Fig. 3-3-3**, **Fig. 3-3-4, Fig. 3-3-5, Fig. 3-3-6**). Furthermore, the CAD-Magnet-Tiam1 system allowed a robust spatial and temporal induction of vertical ruffles on the apical plasma membrane, allowing, in combination with 4D imaging, to study the whole processes in detail (**Fig. 3-3-13**). In contrast, the formation of apical ruffles was not induced with Tiam-pMagFast2(3×). Therefore, the CAD-Magnet system overcomes the limitation of the previous tool and could be applied to more robust induction of previously reported cellular signaling processes, including PI3K[5], trimeric G proteins[6], GEFs[7], cyclins[8].

Previous studies reported several methods to regulate signal transduction via the oligomerization of photoreceptors such as CRY2. For example, LARIAT trap recruits proteins into an oligomer consisting of CRY2 and CIB[9]. This system is able to suppress the cell membrane expansion through trapping small G proteins responsible for actin polymerization. Similarly, IM-LARIAT can induce the inhibition of membrane trafficking through the control of Rab small G proteins[10]. Additionally,

CRY2olig, a point mutation (E490G) of CRY2 resulting in strong homodimerization, effectively induces clustering with target proteins of interest[11]. This method can disrupt the function of clathrin light chain and therefore clathrin-mediated endocytosis of transferrin. The CLICR system can activate receptor tyrosin kinases (RTKs) by clustering through light-induced CRY2 self-oligomerization, inducing cell polarity and lamellipodia extension[12]. However, these previous methods are based on uncontrollable aggregation, which often leads to inefficient performances. Here, I created rational designed-based clustering system. CAD forms a dodecamer complex. Additionally, the Magnet system, based on electrostatic interactions, can avoid unexpected homooligomerization. Furthermore, I can use this system to control signal transduction components, as CAD-Magnet causes no steric hindrance. CAD-Magnet-Tiam1 efficiently induced localized development of membrane ruffles and lamellipodia after blue light irradiation. Therefore, the CAD-Magnet system has potential as a tool to regulate the transduction of other signals as well. The extension of the research to this direction is further tasks in the future.

Apical plasma membrane ruffles are important for macropinocytosis, integrin trafficking, ligand-dependent sequestration and internalization of RTKs, and fast remodeling of the actin cytoskeleton during cell migration and invasion[13–18]. Several types of ruffles, such as dorsal, liner, and circular dorsal ruffles, are dynamically present on the apical plasma membrane[17,19]. For example, the lifetime of circular dorsal

ruffles, the most studied ruffles produced on the apical plasma membrane, is reported to be around 10 minutes[20]. However, the details of ruffle formation dynamics had remained unclear till now. In this study, I revealed the whole apical ruffle formation process (**Fig. 3-3-9**). At first, the ruffle randomly arises from the region irradiated with blue light on the apical plasma membrane to create a wall-shaped formation. The posture gradually shifts to hang over the shape (**Fig. 3-3-13B**, middle panels). After the tip of the ruffle reaches the apical plasma membrane, the ruffle forms a domed structure of less than 5 μm in size (**Fig. 3-3-13B**, top and middle panels). This domed structure lasts for 1 min before the ruffle starts to collapse and fuses with the apical plasma membrane, as if the ruffle engulfs its inner content, before finally disappearing within 1 min. A previous study demonstrated that the iLID system, consisting of Tiam DH/PH domain-SspB and iLID nano-CAAX, could induce the formation of ruffles on the cell edge and lamellipodia. However, this report[21] and other studies[3,22–24] using Tiam did not describe induction of apical ruffle formation. In other words, apical ruffles had not yet been observed even in 2D movies in an inducible way with light. Additionally, apical (dorsal) ruffles are reported mostly as 2D observations using SEM or fluorescence microscopy in studies[14–20], wherein they are induced by addition of growth factor and are not controlled spatiotemporally. Thereby, the origin of ruffle formation and the time of its termination are not speculated by these studies. In the present study, time-lapse 3D (4D) observation of the apical ruffles provides novel

information about the 3D mechanisms underlying formation of apical ruffles, including their origination and termination, because herein ruffle formation is inducible in a spatiotemporally controlled manner. In conclusion, the CAD-Magnet system combined with 4D imaging allowed the first and robust observation of the dynamic 3D processes of ruffle formation in detail. This also demonstrates that CAD-Magnet oligomerizing system is a valuable tool to address specific questions with power and precision.

References

1. Nihongaki, Y., Kawano, F., Nakajima, T. & Sato, M. Photoactivatable CRISPR-Cas9 for optogenetic genome editing. *Nat. Biotechnol.* **33,** 755–760 (2015).

2. Kawano, F., Okazaki, R., Yazawa, M. & Sato, M. A photoactivatable Cre–loxP recombination system for optogenetic genome engineering. *Nat. Chem. Biol.* **12,** 1059–1064 (2016).

3. Kawano, F., Suzuki, H., Furuya, A. & Sato, M. Engineered pairs of distinct photoswitches for optogenetic control of cellular proteins. *Nat. Commun.* **6,** 6256 (2015).

4. Zoltowski, B. D. *et al.* Conformational Switching in the Fungal Light Sensor Vivid. *Science* **316,** 1054–1057 (2007).

5. Idevall-hagren, O., Dickson, E. J., Hille, B., Toomre, D. K. & Camilli, P. De. Optogenetic control of phosphoinositide metabolism. *Proc. Natl. Acad. Sci. U. S. A.* **109,** E2316–E2323 (2012).

6. Yu, G. *et al.* Optical manipulation of the alpha subunits of heterotrimeric G proteins using photoswitchable dimerization systems. *Sci. Rep.* **6,** 35777 (2016).

7. Toettcher, J. E., Weiner, O. D. & Lim, W. A. Using Optogenetics to Interrogate the Dynamic Control of Signal Transmission by the Ras / Erk Module. *Cell* **155,**

1422–1434 (2013).

8. Yang, X., Jost, A. P., Weiner, O. D. & Tang, C. A light-inducible organelle-targeting system for dynamically activating and inactivating signaling in budding yeast. *Mol. Cell. Biol.* **24,** 2419–2430 (2013).

9. Lee, S. *et al.* Reversible protein inactivation by optogenetic trapping in cells. *Nat. Methods* **11,** 633–6 (2014).

10. Nguyen, M. K. *et al.* Optogenetic oligomerization of Rab GTPases regulates intracellular membrane trafficking. *Nat. Chem. Biol.* **12,** 431–436 (2016).

11. Taslimi, A. *et al.* An optimized optogenetic clustering tool for probing protein interaction and function. *Nat. Commun.* **5,** 4925 (2014).

12. Bugaj, L. J. *et al.* Regulation of endogenous transmembrane receptors through optogenetic Cry2 clustering. *Nat. Commun.* **6,** 7898 (2015).

13. Abella, J. V., Parachoniak, C. A., Sangwan, V. & Park, M. Dorsal ruffle microdomains potentiate met receptor tyrosine kinase signaling and down-regulation. *J. Biol. Chem.* **285,** 24956–24967 (2010).

14. Hoon, J.-L., Wong, W.-K. & Koh, C.-G. Functions and regulation of circular dorsal ruffles. *Mol. Cell. Biol.* **32,** 4246–57 (2012).

15. Dowrick, P., Kenworthy, P., McCann, B. & Warn, R. Circular ruffle formation and closure lead to macropinocytosis in hepatocyte growth factor/scatter factor-treated cells. *Eur. J. Cell Biol.* **61,** 44–53 (1993).

16. Gu, Z., Noss, E. H., Hsu, V. W. & Brenner, M. B. Integrins traffic rapidly via circular dorsal ruffles and macropinocytosis during stimulated cell migration. *J. Cell Biol.* **193,** 61–70 (2011).

17. Buccione, R., Orth D., J. & McNiven, M. A. Foot and mouth: podosomes, invadopodia and circular dorsal ruffles. *Nat. Rev. Mol. Cell Biol.* **5,** 647–657 (2004).

18. Orth, J. D. & McNiven, M. A. Get off my back! Rapid receptor internalization through circular dorsal ruffles. *Cancer Res.* **66,** 11094–11096 (2006).

19. Chhabra, E. S. & Higgs, H. N. The many faces of actin: matching assembly factors with cellular structures. *Nat. Cell Biol.* **9,** 1110–1121 (2007).

20. Cortesio L., C., Perrin J., B., Benniin A., D. & Huttenlocher, A. Actin-binding Protein-1 Interacts with WASp-interacting Protein to Regulate Growth Factor-induced Dorsal Ruffle Formation. *Mol. Biol. Cell* **21,** 186–197 (2010).

21. Guntas, G. *et al.* Engineering an improved light-induced dimer (iLID) for controlling the localization and activity of signaling proteins. *Proc. Natl. Acad. Sci.* **112,** 112–117 (2015).

22. Wu, Y. I. *et al.* A genetically encoded photoactivatable Rac controls the motility of living cells. *Nature* **461,** 104–108 (2009).

23. Yazawa, M., Sadaghiani, A. M., Hsueh, B. & Dolmetsch, R. E. Induction of protein-protein interactions in live cells using light. *Nat. Biotechnol.* **27,** 941–945

(2009).

24. Levskaya, A., Weiner, O. D., Lim, W. A. & Voigt, C. A. Spatiotemporal control of cell signalling using a light-switchable protein interaction. *Nature* **461,** 997–1001 (2009).

Appendix

(I) The sequences of the constructs prepared in this study

(i) pMagFast2-mCh-CAD / pcDNA3.1

HindIII
AAGCTT

Kozak sequence
GCCACC

1st Met
ATG

Spacer
GTG

pMagFast2 (VVD-36 I52R/M55R) (450 bp)
CATACTCTTTATGCCCCCGGTGGATATGACATTATGGGATATCTGAGGCAGATCAGGAACCGGCCAAACC
CGCAGGTGGAACTGGGCCCCGTGGATACATCCTGCGCCTTGGTGCTTTGTGACCTGAAACAGAAAGACAC
CCCGGTGGTTTACGCGAGTGAAGCCTTCCTCTACATGACAGGTTACAGCAACGCAGAGGTGCTGGGCCGG
AATTGCCGGTTTCTGCAAAGCCCTGACGGCATGGTGAAGCCCAAGAGCACCCGGAAGTACGTGGATAGTA
ACACAATCAATACTATGCGCAAGGCAATCGACAGGAATGCCGAGGTGCAGGTTGAAGTAGTCAATTTTAA
AAAGAATGGACAGCGATTTGTTAATTTCCTGACTATGATACCTGTTAGGGACGAAACAGGCGAGTATCGA
TACTCTATGGGATTCCAGTGCGAAACAGAA

GS linker (42 base)
GGCGGCAGTGGAGGGTCTGGTGGCAGCGGAGGCGGTTCAGGG

BamHI
GGATCC

mCherry (708 bp)

ATGGTGAGCAAGGGCGAGGAGGATAACATGGCCATCATCAAGGAGTTCATGCGCTTCAAGGTGCACATGG
AGGGCTCCGTGAACGGCCACGAGTTCGAGATCGAGGGCGAGGGCGAGGGCCGCCCCTACGAGGGCACCCA
GACCGCCAAGCTGAAGGTGACCAAGGGTGGCCCCCTGCCCTTCGCCTGGGACATCCTGTCCCCTCAGTTC
ATGTACGGCTCCAAGGCCTACGTGAAGCACCCCGCCGACATCCCCGACTACTTGAAGCTGTCCTTCCCCG
AGGGCTTCAAGTGGGAGCGCGTGATGAACTTCGAGGACGGCGGCGTGGTGACCGTGACCCAGGACTCCTC
CCTGCAGGACGGCGAGTTCATCTACAAGGTGAAGCTGCGCGGCACCAACTTCCCCTCCGACGGCCCCGTA
ATGCAGAAGAAGACCATGGGCTGGGAGGCCTCCTCCGAGCGGATGTACCCCGAGGACGGCGCCCTGAAGG
GCGAGATCAAGCAGAGGCTGAAGCTGAAGGACGGCGGCCACTACGACGCTGAGGTCAAGACCACCTACAA
GGCCAAGAAGCCCGTGCAGCTGCCCGGCGCCTACAACGTCAACATCAAGTTGGACATCACCTCCCACAAC
GAGGACTACACCATCGTGGAACAGTACGAACGCGCCGAGGGCCGCCACTCCACCGGCGGCATGGACGAGC
TGTACAAG

EcoRI

GAATTC

CaMKIIα association domain (a.a.315-478 492 bp)

GGAGGGAAGAGCGGGGGGAACAAGAAGAACGACGGGGTCAAAGAGAGCAGCGAGTCAACCAATACTACAA
TCGAGGACGAAGATACCAAGGTGCGGAAACAGGAGATCATTAAGGTCACCGAGCAGCTGATCGAAGCCAT
TTCTAACGGGGACTTCGAAAGTTACACAAAAATGTGCGATCCCGGAATGACTGCATTTGAGCCTGAAGCC
CTGGGAAATCTGGTGGAGGGCCTGGACTTCCACCGATTCTATTTTGAAAACCTGTGGAGCAGAAATTCCA
AGCCAGTCCATACCACAATCCTGAACCCCCACATTCATCTGATGGGCGACGAGAGCGCCTGTATCGCTTA
CATCCGGATTACACAGTATCTGGATGCTGGCGGGATTCCCAGGACTGCACAGTCTGAGGAAACCCGCGTG
TGGCACCGGAGAGATGGGAAATGGCAGATTGTCCACTTTCACAGAAGCGGAGCACCAAGCGTCCTGCCTC
AT

STOP

TGA

XhoI
CTCGAG

[amino sequence]

MVHTLYAPGGYDIMGYLRQIRNRPNPQVELGPVDTSCALVLCDLKQKDTPVVYASEAFLYMTGYSNAEVL
GRNCRFLQSPDGMVKPKSTRKYVDSNTINTMRKAIDRNAEVQVEVVNFKKNGQRFVNFLTMIPVRDETGE
YRYSMGFQCETEGGSGGSGGSGGGSGGSMVSKGEEDNMAIIKEFMRFKVHMEGSVNGHEFEIEGEGEGRP
YEGTQTAKLKVTKGGPLPFAWDILSPQFMYGSKAYVKHPADIPDYLKLSFPEGFKWERVMNFEDGGVVTV
TQDSSLQDGEFIYKVKLRGTNFPSDGPVMQKKTMGWEASSERMYPEDGALKGEIKQRLKLKDGGHYDAEV
KTTYKAKKPVQLPGAYNVNIKLDITSHNEDYTIVEQYERAEGRHSTGGMDELYKEFGGKSGGNKKNDGVK
ESSESTNTTIEDEDTKVRKQEIIKVTEQLIEAISNGDFESYTKMCDPGMTAFEPEALGNLVEGLDFHRFY
FENLWSRNSKPVHTTILNPHIHLMGDESACIAYIRITQYLDAGGIPRTAQSEETRVWHRRDGKWQIVHFH
RSGAPSVLPH*

(ii) Lifeact-mCh-P2A-Tiam1 DH/PH domain-pMagFast2-CAD /pcDNA3.1

HindIII
AAGCTT

Kz sequence
GCCACC

Lifeact (51 base)
ATGGGCGTGGCCGACCTGATCAAGAAGTTCGAGAGCATCAGCAAGGAGGAG

linker (21 base)
GGCGACCCACCTGTGGCCACC

mCherry (708 base)

ATGGTGAGCAAGGGCGAGGAGGATAACATGGCCATCATCAAGGAGTTCATGCGCTTCAAGGTGCACATGG
AGGGCTCCGTGAACGGCCACGAGTTCGAGATCGAGGGCGAGGGCGAGGGCCGCCCCTACGAGGGCACCCA
GACCGCCAAGCTGAAGGTGACCAAGGGTGGCCCCCTGCCCTTCGCCTGGGACATCCTGTCCCCTCAGTTC
ATGTACGGCTCCAAGGCCTACGTGAAGCACCCCGCCGACATCCCCGACTACTTGAAGCTGTCCTTCCCCG
AGGGCTTCAAGTGGGAGCGCGTGATGAACTTCGAGGACGGCGGCGTGGTGACCGTGACCCAGGACTCCTC
CCTGCAGGACGGCGAGTTCATCTACAAGGTGAAGCTGCGCGGCACCAACTTCCCCTCCGACGGCCCCGTA
ATGCAGAAGAAGACCATGGGCTGGGAGGCCTCCTCCGAGCGGATGTACCCCGAGGACGGCGCCCTGAAGG
GCGAGATCAAGCAGAGGCTGAAGCTGAAGGACGGCGGCCACTACGACGCTGAGGTCAAGACCACCTACAA
GGCCAAGAAGCCCGTGCAGCTGCCCGGCGCCTACAACGTCAACATCAAGTTGGACATCACCTCCCACAAC
GAGGACTACACCATCGTGGAACAGTACGAACGCGCCGAGGGCCGCCACTCCACCGGCGGCATGGACGAGC
TGTACAAG

BamHI

GGATCC

P2A peptide (66 base)

GGCAGCGGCGCCACCAACTTCAGCCTGCTGAAGCAGGCCGGCGACGTGGAGGAGAACCCCGGCCCC

XbaI/NheI

TCTAGC

Kozak sequence

GCC ACC

Start codon

ATG

Spacer

GTG

Tiam1 DH/PH domain (1,122 base)

CGACAGCTGTCGGATGCGGATAAGCTGCGCAAGGTGATCTGTGAACTGCTGGAGACTGAACGCACCTATG
TGAAAGACTTAAACTGCCTCATGGAGAGATACCTGAAGCCCCTTCAGAAGGAGACCTTTCTCACCCAGGA
TGAGCTTGATGTACTTTTTGGAAATTTAACCGAAATGGTGGAGTTTCAAGTCGAGTTCCTTAAGACTCTG
GAAGATGGAGTAAGACTGGTCCCTGACTTGGAAAAGCTGGAGAAGGTTGACCAGTTCAAGAAAGTGCTCT
TCTCTCTGGGGGGCTCCTTCCTGTACTACGCGGACCGCTTCAAGCTCTACAGTGCCTTCTGTGCGAGCCA
CACAAAAGTCCCCAAGGTCCTGGTGAAAGCCAAGACGGACACAGCCTTCAAGGCGTTCCTCGATGCCCAG
AACCCGAGGCAGCAGCACTCATCCACGCTGGAGTCTTACCTCATCAAGCCCATCCAGAGGGTCCTCAAGT
ACCCGCTTCTGCTCAGGGAGCTGTTTGCGCTGACCGATGCGGAGAGCGAGGAACACTACCACCTGGACGT
GGCCATCAAGACTATGAACAAGGTCGCCAGTCACATCAATGAGATGCAGAAGATCCACGAAGAGTTTGGT
GCTGTGTTTGACCAGCTGATTGCTGAGCAGACGGGAGAGAAGAAAGAGGTTGCAGATCTGAGCATGGGTG
ACCTGCTCTTGCACACCAGCGTCATCTGGCTGAACCCACCCGCCTCACTGGGAAAGTGGAAAAAGGAGCC
AGAATTAGCAGCCTTCGTCTTCAAAACGGCCGTGGTCCTTGTATATAAAGACGGTTCCAAGCAGAAGAAG
AAACTTGTTGGCTCTCACAGGCTGTCAATCTACGAGGAGTGGGACCCTTTCCGGTTTCGCCACATGATCC
CTACCGAAGCCTTGCAGGTCCGAGCTCTGCCCAGTGCAGATGCAGAGGCAAATGCGGTATGCGAAATTGT
CCACGTGAAATCAGAGTCAGAAGGGAGGCCCGAGCGGGTTTTCCACCTCTGCTGCAGTTCCCCAGAGAGC
AGAAAGGACTTTCTGAAGTCTGTGCATTCGATCCTGCGAGATAAACACAGAAGACAGCTCCTCAAAACGG
AA

GS linker (60 base)

GGCGGTGGAAGTGGTGGAGGTTCTGGGGGCTCCGGAGGTAGCGGTGGAGGCTCAGGTGGA

HindIII

AAGCTT

Spacer

GGCGGA

pMagFast2 (VVD-36 I52R/M55R) (450 bp)

CATACTCTTTATGCCCCCGGTGGATATGACATTATGGGATATCTGAGGCAGATCAGGAACCGGCCAAACC
CGCAGGTGGAACTGGGCCCCGTGGATACATCCTGCGCCTTGATTCTTTGTGACCTGAAACAGAAAGACAC
CCCGATAGTTTACGCGAGTGAAGCCTTCCTCTACATGACAGGTTACAGCAACGCAGAGGTGCTGGGCCGG
AATTGCCGGTTTCTGCAAAGCCCTGACGGCATGGTGAAGCCCAAGAGCACCCGGAAGTACGTGGATAGTA
ACACAATCAATACTATGCGCAAGGCAATCGACAGGAATGCCGAGGTGCAGGTTGAAGTAGTCAATTTTAA
AAAGAATGGACAGCGATTTGTTAATTTCCTGACTATGATACCTGTTAGGGACGAAACAGGCGAGTATCGA
TACTCTATGGGATTCCAGTGCGAAACAGAA

BamHI

GGATCC

Kozak sequence

GCCACC

Start codon

ATG

CaMKIIα association domain (a.a.315-478 492 bp)

GGAGGGAAGAGCGGGGGGAACAAGAAGAACGACGGGGTCAAAGAGAGCAGCGAGTCAACCAATACTACAA
TCGAGGACGAAGATACCAAGGTGCGGAAACAGGAGATCATTAAGGTCACCGAGCAGCTGATCGAAGCCAT
TTCTAACGGGGACTTCGAAAGTTACACAAAAATGTGCGATCCCGGAATGACTGCATTTGAGCCTGAAGCC
CTGGGAAATCTGGTGGAGGGCCTGGACTTCCACCGATTCTATTTTGAAAACCTGTGGAGCAGAAATTCCA
AGCCAGTCCATACCACAATCCTGAACCCCCACATTCATCTGATGGGCGACGAGAGCGCCTGTATCGCTTA
CATCCGGATTACACAGTATCTGGATGCTGGCGGGATTCCCAGGACTGCACAGTCTGAGGAAACCCGCGTG
TGGCACCGGAGAGATGGGAAATGGCAGATTGTCCACTTTCACAGAAGCGGAGCACCAAGCGTCCTGCCTC
AT

STOP

TAA

XhoI
CTCGAG

[amino sequence]

(Lifeact-mCh)
MGVADLIKKFESISKEEGDPPVATMVSKGEEDNMAIIKEFMRFKVHMEGSVNGHEFEIEGEGEGRPYEGT
QTAKLKVTKGGPLPFAWDILSPQFMYGSKAYVKHPADIPDYLKLSFPEGFKWERVMNFEDGGVVTVTQDS
SLQDGEFIYKVKLRGTNFPSDGPVMQKKTMGWEASSERMYPEDGALKGEIKQRLKLKDGGHYDAEVKTTY
KAKKPVQLPGAYNVNIKLDITSHNEDYTIVEQYERAEGRHSTGGMDELYKGSGSGATNFSLLKQAGDVEE
NPG
(Tiam1 DH/PH domain-pMagFast2-CAD)
PSSATMVRQLSDADKLRKVICELLETERTYVKDLNCLMERYLKPLQKETFLTQDELDVLFGNLTEMVEFQ
VEFLKTLEDGVRLVPDLEKLEKVDQFKKVLFSLGGSFLYYADRFKLYSAFCASHTKVPKVLVKAKTDTAF
KAFLDAQNPRQQHSSTLESYLIKPIQRVLKYPLLLRELFALTDAESEEHYHLDVAIKTMNKVASHINEMQ
KIHEEFGAVFDQLIAEQTGEKKEVADLSMGDLLLHTSVIWLNPPASLGKWKKEPELAAFVFKTAVVLVYK
DGSKQKKKLVGSHRLSIYEEWDPFRFRHMIPTEALQVRALPSADAEANAVCEIVHVKSESEGRPERVFHL
CCSSPESRKDFLKSVHSILRDKHRRQLLKTEGGGSGGGSGGSGGSGGGSGGKLGGHTLYAPGGYDIMGYL
RQIRNRPNPQVELGPVDTSCALILCDLKQKDTPIVYASEAFLYMTGYSNAEVLGRNCRFLQSPDGMVKPK
STRKYVDSNTINTMRKAIDRNAEVQVEVVNFKKNGQRFVNFLTMIPVRDETGEYRYSMGFQCETEGSATM
GGKSGGNKKNDGVKESSESTNTTIEDEDTKVRKQEIIKVTEQLIEAISNGDFESYTKMCDPGMTAFEPEA
LGNLVEGLDFHRFYFENLWSRNSKPVHTTILNPHIHLMGDESACIAYIRITQYLDAGGIPRTAQSEETRV
WHRRDGKWQIVHFHRSGAPSVLPH*

(iii) Lifeact-mCh-P2A-Tiam1 DH/PH domain-pMagFast2(3×) /pcDNA3.1

HindIII
AAGCTT

Kz sequence

GCCACC

Lifeact (51 base)

ATGGGCGTGGCCGACCTGATCAAGAAGTTCGAGAGCATCAGCAAGGAGGAG

linker (21 base)

GGCGACCCACCTGTGGCCACC

mCherry (708 base)

ATGGTGAGCAAGGGCGAGGAGGATAACATGGCCATCATCAAGGAGTTCATGCGCTTCAAGGTGCACATGG
AGGGCTCCGTGAACGGCCACGAGTTCGAGATCGAGGGCGAGGGCGAGGGCCGCCCCTACGAGGGCACCCA
GACCGCCAAGCTGAAGGTGACCAAGGGTGGCCCCCTGCCCTTCGCCTGGGACATCCTGTCCCCTCAGTTC
ATGTACGGCTCCAAGGCCTACGTGAAGCACCCCGCCGACATCCCCGACTACTTGAAGCTGTCCTTCCCCG
AGGGCTTCAAGTGGGAGCGCGTGATGAACTTCGAGGACGGCGGCGTGGTGACCGTGACCCAGGACTCCTC
CCTGCAGGACGGCGAGTTCATCTACAAGGTGAAGCTGCGCGGCACCAACTTCCCCTCCGACGGCCCCGTA
ATGCAGAAGAAGACCATGGGCTGGGAGGCCTCCTCCGAGCGGATGTACCCCGAGGACGGCGCCCTGAAGG
GCGAGATCAAGCAGAGGCTGAAGCTGAAGGACGGCGGCCACTACGACGCTGAGGTCAAGACCACCTACAA
GGCCAAGAAGCCCGTGCAGCTGCCCGGCGCCTACAACGTCAACATCAAGTTGGACATCACCTCCCACAAC
GAGGACTACACCATCGTGGAACAGTACGAACGCGCCGAGGGCCGCCACTCCACCGGCGGCATGGACGAGC
TGTACAAG

BamHI

GGATCC

P2A peptide (66 base)

GGCAGCGGCGCCACCAACTTCAGCCTGCTGAAGCAGGCCGGCGACGTGGAGGAGAACCCCGGCCCC

XbaI/NheI

TCTAGC

Kozak sequence

GCC ACC

Start codon

ATG

Spacer

GTG

Tiam1 DH/PH domain (1,122 base)

CGACAGCTGTCGGATGCGGATAAGCTGCGCAAGGTGATCTGTGAACTGCTGGAGACTGAACGCACCTATG
TGAAAGACTTAAACTGCCTCATGGAGAGATACCTGAAGCCCCTTCAGAAGGAGACCTTTCTCACCCAGGA
TGAGCTTGATGTACTTTTTGGAAATTTAACCGAAATGGTGGAGTTTCAAGTCGAGTTCCTTAAGACTCTG
GAAGATGGAGTAAGACTGGTCCCTGACTTGGAAAAGCTGGAGAAGGTTGACCAGTTCAAGAAAGTGCTCT
TCTCTCTGGGGGGCTCCTTCCTGTACTACGCGGACCGCTTCAAGCTCTACAGTGCCTTCTGTGCGAGCCA
CACAAAAGTCCCCAAGGTCCTGGTGAAAGCCAAGACGGACACAGCCTTCAAGGCGTTCCTCGATGCCCAG
AACCCGAGGCAGCAGCACTCATCCACGCTGGAGTCTTACCTCATCAAGCCCATCCAGAGGGTCCTCAAGT
ACCCGCTTCTGCTCAGGGAGCTGTTTGCGCTGACCGATGCGGAGAGCGAGGAACACTACCACCTGGACGT
GGCCATCAAGACTATGAACAAGGTCGCCAGTCACATCAATGAGATGCAGAAGATCCACGAAGAGTTTGGT
GCTGTGTTTGACCAGCTGATTGCTGAGCAGACGGGAGAGAAGAAAGAGGTTGCAGATCTGAGCATGGGTG
ACCTGCTCTTGCACACCAGCGTCATCTGGCTGAACCCACCCGCCTCACTGGGAAAGTGGAAAAAGGAGCC
AGAATTAGCAGCCTTCGTCTTCAAAACGGCCGTGGTCCTTGTATATAAAGACGGTTCCAAGCAGAAGAAG
AAACTTGTTGGCTCTCACAGGCTGTCAATCTACGAGGAGTGGGACCCTTTCCGGTTTCGCCACATGATCC
CTACCGAAGCCTTGCAGGTCCGAGCTCTGCCCAGTGCAGATGCAGAGGCAAATGCGGTATGCGAAATTGT
CCACGTGAAATCAGAGTCAGAAGGGAGGCCCGAGCGGGTTTTCCACCTCTGCTGCAGTTCCCCAGAGAGC
AGAAAGGACTTTCTGAAGTCTGTGCATTCGATCCTGCGAGATAAACACAGAAGACAGCTCCTCAAAACGG
AA

GS linker (60 base)

GGCGGTGGAAGTGGTGGAGGTTCTGGGGGCTCCGGAGGTAGCGGTGGAGGCTCAGGTGGA

HindIII

AAGCTT

Spacer

GGCGGA

1st pMagFast2

CACACACTGTATGCTCCAGGCGGCTACGACATCATGGGGTATCTGAGGCAGATTAGGAATAGACCAAATC
CTCAGGTGGAGCTGGGACCTGTGGACACAAGCTGCGCCCTGGTGCTGTGTGACCTGAAGCAGAAAGATAC
CCCTGTGGTCTACGCCAGCGAGGCTTTCCTGTACATGACAGGGTATTCCAACGCTGAAGTGCTGGGACGA
AATTGCCGGTTTCTGCAGTCCCCCGATGGGATGGTGAAGCCTAAATCAACTAGGAAGTATGTGGACAGCA
ACACCATCAATACAATGCGGAAAGCCATTGATAGAAACGCTGAGGTGCAGGTCGAAGTGGTCAACTTCAA
GAAAAATGGCCAGCGCTTCGTGAATTTTCTGACCATGATCCCCGTCAGAGACGAGACAGGCGAATACAGG
TATTCCATGGGGTTTCAGTGTGAGACTGAG

GS linker

GGAGGGAGCGGAGGCTCCGGAGGAGGCTCT

2nd pMagFast2

CACACCCTGTATGCACCTGGGGGATATGACATCATGGGCTACCTGAGACAGATTCGGAACAGACCAAATC
CCCAGGTGGAGCTGGGACCAGTCGATACCTCTTGCGCACTGGTCCTGTGCGACCTGAAACAGAAGGATAC
ACCCGTGGTCTACGCATCTGAGGCCTTCCTGTACATGACTGGCTATAGTAACGCCGAAGTGCTGGGGAGA
AATTGCAGGTTTCTGCAGAGTCCAGACGGCATGGTGAAGCCCAAATCCACACGGAAGTATGTGGACTCTA
ACACTATCAATACCATGAGGAAAGCAATTGATCGCAACGCCGAAGTCCAGGTGGAGGTCGTGAATTTTAA
GAAAAATGGCCAGAGATTCGTGAATTTTCTGACTATGATTCCAGTCCGCGATGAGACCGGAGAATACCGA
TATAGTATGGGCTTTCAGTGTGAAACAGAG

GS linker
GGAGGGTCTGGAGGCAGTGGAGGAGGCTCA

3rd pMagFast2
CATACACTGTATGCCCCCGGGGGATACGACATCATGGGCTATCTGCGGCAGATTAGGAACCGCCCTAATC
CACAGGTGGAGCTGGGGCCTGTCGATACCAGCTGCGCTCTGGTCCTGTGTGACCTGAAACAGAAAGATAC
TCCAGTGGTCTACGCTTCAGAGGCATTCCTGTACATGACCGGATATAGCAACGCCGAAGTGCTGGGCCGC
AATTGCCGATTTCTGCAGTCCCCTGACGGCATGGTGAAGCCAAAAAGTACCAGGAAGTACGTGGACTCAA
ACACAATCAATACTATGCGAAAGGCTATTGATCGGAACGCAGAAGTCCAGGTGGAGGTGGTGAATTTCAA
GAAAAATGGACAGCGCTTCGTGAACTTTCTGACAATGATCCCTGTCCGGGATGAGACTGGCGAATACAGA
TACAGTATGGGCTTCCAGTGCGAGACAGAG

STOP
TAA

XhoI
CTCGAG

[amino sequence]

(Lifeact-mCh)
MGVADLIKKFESISKEEGDPPVATMVSKGEEDNMAIIKEFMRFKVHMEGSVNGHEFEIEGEGEGRPYEGT
QTAKLKVTKGGPLPFAWDILSPQFMYGSKAYVKHPADIPDYLKLSFPEGFKWERVMNFEDGGVVTVTQDS
SLQDGEFIYKVKLRGTNFPSDGPVMQKKTMGWEASSERMYPEDGALKGEIKQRLKLKDGGHYDAEVKTTY
KAKKPVQLPGAYNVNIKLDITSHNEDYTIVEQYERAEGRHSTGGMDELYKGSGSGATNFSLLKQAGDVEE
NPG
(Tiam1 DH/PH domain-pMagFast2(3x))
PSSATMVRQLSDADKLRKVICELLETERTYVKDLNCLMERYLKPLQKETFLTQDELDVLFGNLTEMVEFQ
VEFLKTLEDGVRLVPDLEKLEKVDQFKKVLFSLGGSFLYYADRFKLYSAFCASHTKVPKVLVKAKTDTAF
KAFLDAQNPRQQHSSTLESYLIKPIQRVLKYPLLLRELFALTDAESEEHYHLDVAIKTMNKVASHINEMQ
KIHEEFGAVFDQLIAEQTGEKKEVADLSMGDLLLHTSVIWLNPPASLGKWKKEPELAAFVFKTAVVLVYK

DGSKQKKKLVGSHRLSIYEEWDPFRFRHMIPTEALQVRALPSADAEANAVCEIVHVKSESEGRPERVFHL
CCSSPESRKDFLKSVHSILRDKHRRQLLKTEGGGSGGGSGGSGGSGGGSGGKLGGHTLYAPGGYDIMGYL
RQIRNRPNPQVELGPVDTSCALVLCDLKQKDTPVVYASEAFLYMTGYSNAEVLGRNCRFLQSPDGMVKPK
STRKYVDSNTINTMRKAIDRNAEVQVEVVNFKKNGQRFVNFLTMIPVRDETGEYRYSMGFQCETEGGSGG
SGGGSHTLYAPGGYDIMGYLRQIRNRPNPQVELGPVDTSCALVLCDLKQKDTPVVYASEAFLYMTGYSNA
EVLGRNCRFLQSPDGMVKPKSTRKYVDSNTINTMRKAIDRNAEVQVEVVNFKKNGQRFVNFLTMIPVRDE
TGEYRYSMGFQCETEGGSGGSGGGSHTLYAPGGYDIMGYLRQIRNRPNPQVELGPVDTSCALVLCDLKQK
DTPVVYASEAFLYMTGYSNAEVLGRNCRFLQSPDGMVKPKSTRKYVDSNTINTMRKAIDRNAEVQVEVVN
FKKNGQRFVNFLTMIPVRDETGEYRYSMGFQCETE*

(iv) nMagHigh1-EGFP-CAAX(KRas) / pcDNA3.1-WPRE-pA

EcoRI
GAATTC

Kozak sequence
GCCACC

1st Met
ATG

Spacer
GGA

nMagHigh1 (VVD-36 I52D/M55G/M135I/M165I)(450 base)
CATACTCTTTATGCCCCCGGTGGATATGACATTATGGGATATCTGGACCAGATCGGCAACCGGCCAAACC
CGCAGGTGGAACTGGGCCCCGTGGATACATCCTGCGCCTTGATTCTTTGTGACCTGAAACAGAAAGACAC
CCCGATAGTTTACGCGAGTGAAGCCTTCCTCTACATGACAGGTTACAGCAACGCAGAGGTGCTGGGCCGG
AATTGCCGGTTTCTGCAAAGCCCTGACGGCATGGTGAAGCCCAAGAGCACCCGGAAGTACGTGGATAGTA

ACACAATCAATACTATCCGCAAGGCAATCGACAGGAATGCCGAGGTGCAGGTTGAAGTAGTCAATTTTAA
AAAGAATGGACAGCGATTTGTTAATTTCCTGACTATCATACCTGTTAGGGACGAAACAGGCGAGTATCGA
TACTCTATGGGATTCCAGTGCGAAACAGAA

GS linker (42 base)
GGCGGTAGCGGAGGCTCTGGTGGAAGCGGTGGCAGCGGCGGT

BamHI
GGATCC

EGFP (720 bp)
ATGGTGAGCAAGGGCGAGGAGCTGTTCACCGGGGTGGTGCCCATCCTGGTCGAGCTGGACGGCGACGTAA
ACGGCCACAAGTTCAGCGTGTCCGGCGAGGGCGAGGGCGATGCCACCTACGGCAAGCTGACCCTGAAGTT
CATCTGCACCACCGGCAAGCTGCCCGTGCCCTGGCCCACCCTCGTGACCACCCTGACCTACGGCGTGCAG
TGCTTCAGCCGCTACCCCGACCACATGAAGCAGCACGACTTCTTCAAGTCCGCCATGCCCGAAGGCTACG
TCCAGGAGCGCACCATCTTCTTCAAGGACGACGGCAACTACAAGACCCGCGCCGAGGTGAAGTTCGAGGG
CGACACCCTGGTGAACCGCATCGAGCTGAAGGGCATCGACTTCAAGGAGGACGGCAACATCCTGGGGCAC
AAGCTGGAGTACAACTACAACAGCCACAACGTCTATATCATGGCCGACAAGCAGAAGAACGGCATCAAGG
TGAACTTCAAGATCCGCCACAACATCGAGGACGGCAGCGTGCAGCTCGCCGACCACTACCAGCAGAACAC
CCCCATCGGCGACGGCCCCGTGCTGCTGCCCGACAACCACTACCTGAGCACCCAGTCCGCCCTGAGCAAA
GACCCCAACGAGAAGCGCGATCACATGGTCCTGCTGGAGTTCGTGACCGCCGCCGGGATCACTCTCGGCA
TGGACGAGCTGTATAAGGGT

CAAX (K-Ras 4B)(42 base)
AAAAAGAAGAAAAAGAAGTCAAAGACAAAGTGTGTAATTATG

STOP
TAG

Space (22 base)
CTGTACAAGTCCGGACTCAGAT

XhoI
CTCGAG

XbaI
TCTAGA

STOP codon
TGA

WPRE (588 base)
TCAACCTCTGGATTACAAAATTTGTGAAAGATTGACTGGTATTCTTAACTATGTTGCTCCTTTTACGCTA
TGTGGATACGCTGCTTTAATGCCTTTGTATCATGCTATTGCTTCCCGTATGGCTTTCATTTTCTCCTCCT
TGTATAAATCCTGGTTGCTGTCTCTTTATGAGGAGTTGTGGCCCGTTGTCAGGCAACGTGGCGTGGTGTG
CACTGTGTTTGCTGACGCAACCCCCACTGGTTGGGGCATTGCCACCACCTGTCAGCTCCTTTCCGGGACT
TTCGCTTTCCCCCTCCCTATTGCCACGGCGGAACTCATCGCCGCCTGCCTTGCCCGCTGCTGGACAGGGG
CTCGGCTGTTGGGCACTGACAATTCCGTGGTGTTGTCGGGGAAGCTGACGTCCTTTCCATGGCTGCTCGC
CTGTGTTGCCACCTGGATTCTGCGCGGGACGTCCTTCTGCTACGTCCCTTCGGCCCTCAATCCAGCGGAC
CTTCCTTCCCGCGGCCTGCTGCCGGCTCTGCGGCCTCTTCCGCGTCTTCGCCTTCGCCCTCAGACGAGTC
GGATCTCCCTTTGGGCCGCCTCCCCGCA

Spacer
TCGGTACAA

pA (527 base)
TTCACTCCTCAGGTGCAGGCTGCCTATCAGAAGGTGGTGGCTGGTGTGGCCAATGCCCTGGCTCACAAAT
ACCACTGAGATCTTTTTCCCTCTGCCAAAAATTATGGGGACATCATGAAGCCCCTTGAGCATCTGACTTC
TGGCTAATAAAGGAAATTTATTTTCATTGCAATAGTGTGTTGGAATTTTTTGTGTCTCTCACTCGGAAGG

ACATATGGGAGGGCAAATCATTTAAAACATCAGAATGAGTATTTGGTTTAGAGTTTGGCAACATATGCCC
ATATGCTGGCTGCCATGAACAAAGGTTGGCTATAAAGAGGTCATCAGTATATGAAACAGCCCCCTGCTGT
CCATTCCTTATTCCATAGAAAAGCCTTGACTTGAGGTTAGATTTTTTTTATATTTTGTTTTGTGTTATTT
TTTTCTTTAACATCCCTAAAATTTTCCTTACATGTTTTACTAGCCAGATTTTTCCTCCTCTCCTGACTAC
TCCCAGTCATAGCTGTCCCTCTTCTCTTATGGAGATC

ApaI
GGGCCC

[amino sequence]

MGHTLYAPGGYDIMGYLDQIGNRPNPQVELGPVDTSCALILCDLKQKDTPIVYASEAFLYMTGYSNAEVL
GRNCRFLQSPDGMVKPKSTRKYVDSNTINTIRKAIDRNAEVQVEVVNFKKNGQRFVNFLTIIPVRDETGE
YRYSMGFQCETEGGSGGSGGSGGSGGGSMVSKGEELFTGVVPILVELDGDVNGHKFSVSGEGEGDATYGK
LTLKFICTTGKLPVPWPTLVTTLTYGVQCFSRYPDHMKQHDFFKSAMPEGYVQERTIFFKDDGNYKTRAE
VKFEGDTLVNRIELKGIDFKEDGNILGHKLEYNYNSHNVYIMADKQKNGIKVNFKIRHNIEDGSVQLADH
YQQNTPIGDGPVLLPDNHYLSTQSALSKDPNEKRDHMVLLEFVTAAGITLGMDELYKGKKKKKKSKTKCV
IM*

(II) The structure of the vector used in this study

[pcDNA3.1]

I only used pcDNA3.1(+) for constructs prepared in this study. I describe its structure below.

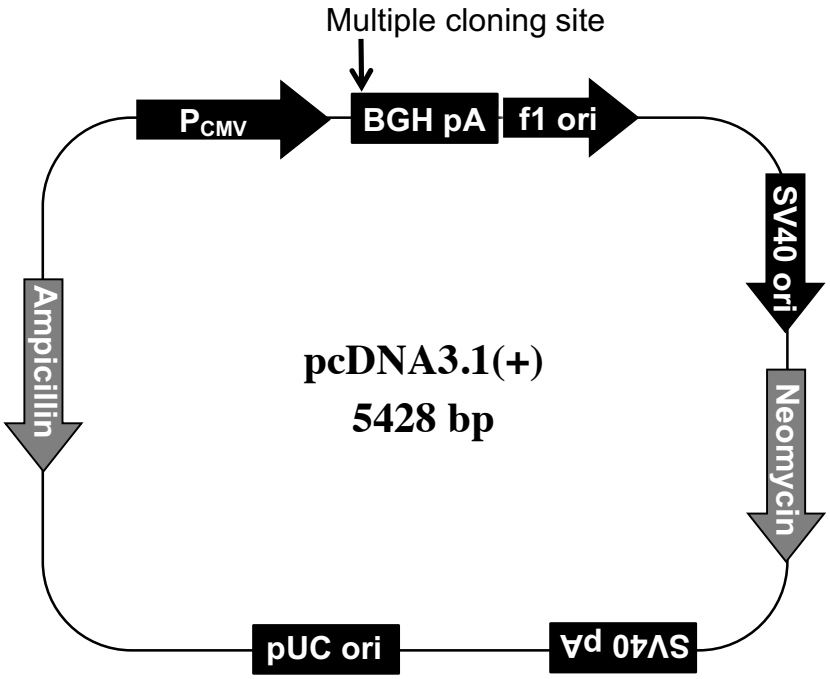

CMV promoter: bases 232-819
T7 promoter/priming site: bases 863-882
Multiple cloning site: bases 895-1010
pcDNA3.1/BGH reverse priming site: bases 1022-1039
BGH polyadenylation sequence: bases 1028-1252
f1 origin: bases 1298-1726
SV40 early promoter and origin: bases 1731-2074
Neomycin resistance gene (ORF): bases 2136-2930
SV40 early polyadenylation signal: bases 3104-3234
pUC origin: bases 3617-4287 (complementary strand)
Ampicillin resistance gene (*bla*): bases 4432-5428 (complementary strand)
ORF: bases 4432-5292 (complementary strand)
Ribosome binding site: bases 5300-5304 (complementary strand)
bla promoter (P3): bases 5327-5333 (complementary strand)

The sequence of Multiple cloning site of pcDNA3.1(+) (bases 895-1010)

```
         NheI                 HindIII         KpnI     BamHI
          |                     |               |        |
891 GCTGGCTAGC GTTTAAACTT AAGCTTGGTA CCGAGCTCGG ATCCACTAGT CCAGTGTGGT

      EcoRI          EcoRV                      XhoI     XbaI         ApaI
       |              |                          |        |            |
951 GGAATTCTGC AGATATCCAG CACAGTGGCG GCCGCTCGAG TCTAGAGGGC CCGTTTAAAC
```

Constructs (i), (ii), (iii) in the last section were inserted between *Hind*III and *Xho*I. Construct (iv) was inserted between *Eco*RI and *Apa*I.